6 Multiple Scattering: Advanced

The theory of reflection, transmission, and absorption by a pile of discrete plates, and the two-stream theory for a continuous medium, discussed in the previous chapter, are so mathematically simple and physically transparent that from them you can acquire most of the physical understanding and insight you'll ever need. But sometimes you do need more accurate numbers than these theories can provide. Moreover, the two-stream theory is incapable of accounting for the full directionality of the radiation field. The next step is to generalize from 2 to N streams, which may lead to greater accuracy but at the expense of greater complexity. In the limit as N approaches infinity, we obtain the integro-differential equation of radiative transfer, which is exact (subject to underlying approximations and assumptions). A staggering number of mathematical methods for solving this equation, mostly for plane-parallel media (which don't exist), have been confected, all of them complex, some of them obsolete. We could fill a thick volume with mathematical methods and computations comparing (to nine digits) the results of one method with those of another. But to what end? Instead of drowning in a sea of methods, we consider only two: diffusion theory and the Monte Carlo method. Diffusion theory is the simplest analytical means for escaping from the one-dimensional prison of plane-parallel media. The Monte Carlo method can treat complex, finite, inhomogeneous media with irregular boundaries – the kinds of media that are the rule in Nature.

6.1 N-Stream Theory and Beyond

Equations (5.40) and (5.41) can be written more compactly as a single equation:

$$\mu_k \frac{dF_k}{dz} = -(\kappa + \beta)F_k + \beta \sum_{j=1}^{2} p_{jk} F_j, \ k = 1, 2, \tag{6.1}$$

where p_{jk} is the probability that a photon in the direction j is scattered in the direction k. Here j and k take on only two values: 1 corresponds to downward, 2 corresponds to upward. The quantity μ_k, the cosine of the angle between the positive z-axis and either of the two allowed directions, takes on only two values, 1 and -1.

This immediately suggests generalizing the two-stream theory to N streams:

$$\mu_k \frac{dF_k}{dz} = -(\kappa + \beta)F_k + \beta \sum_{j=1}^{N} q_{jk} F_j, \ k = 1, 2, \ldots, N, \tag{6.2}$$

Fundamentals of Atmospheric Radiation: An Introduction with 400 Problems. Craig F. Bohren and Eugene E. Clothiaux

ISBN: 3-527-40503-8

where

$$q_{jk} = \pm p_{jk} \left(\frac{\mu_k}{\mu_j} \right). \tag{6.3}$$

Here p_{jk} is the probability that, given that a photon in direction j is scattered, it is scattered in direction k; the μ_k are direction cosines. The symbol $\pm$ indicates that the sign is chosen to make the entire quantity positive (as it must be). The radiation field is approximated as a set of monodirectional beams, each with zero angular divergence, which, of course, is not possible. Even a laser beam has a small angular divergence. In the N-stream theory we make some assumptions we know are not true. For example, we assume that p_{jk} is the probability that a photon in direction j is scattered into direction k. Such a probability does not strictly exist. Or perhaps we should say that the probability of scattering exactly in one direction is zero because scattering directions (as far as we know) vary continuously. The correct probability is a distribution function giving the probability of scattering into a finite, although possibly small, set of directions (i.e., small solid angle). Note also that if we were to choose one of our directions to be 90°, we'd end up with an infinite quantity in the equation of transfer. In the derivation we assume (strictly) that $\beta \Delta z/\mu \ll 1$. Here $\Delta z/\mu$ is the distance along a particular direction. When $\mu = 0$, this condition cannot be satisfied. The idealizations and approximations that go into the N-stream theory underscore why we have to go beyond it. The right side of Eq. (6.2) is a sum. An integral is the limit of a sum as the number of terms in it goes to infinity. This suggests that an integral will appear in the equation of transfer, which we turn to after making a brief detour to discuss the directional derivative.

6.1.1 Directional Derivative

First consider a function f of a single variable, call it x. The values of x can be represented by points on a line. The derivative of f is defined as

$$\frac{df}{dx} = \lim_{\Delta x \to 0} \frac{f(x + \Delta x) - f(x)}{\Delta x} \tag{6.4}$$

provided this limit exists. The numerator and denominator separately have the limit zero but the limit of their quotient is not necessarily zero. Note that the derivative is *not* the quotient df over dx; this is just a symbol that reminds us how the derivative is defined. The number of possible symbols is indefinite. For example, we could write the derivative as f', a different symbol with the same meaning.

The derivative Eq. (6.4) is, in fact, a *directional derivative*, although rarely called such. It is the rate of change of f along a particular direction (the x-axis). Here there is only one direction, so it is not necessary to call this derivative a directional derivative. What happens, however, when f is defined for points $\mathbf{x}$ in three-dimensional space? Here we have an infinite number of possibilities for the rate of change of f depending on direction. A direction can be specified by a unit vector $\mathbf{\Omega}$. Thus the value of the function f at a distance s from x along the direction $\mathbf{\Omega}$ is $f(x + s\mathbf{\Omega})$, and hence the rate of change of f with distance along this direction is

$$\frac{f(\mathbf{x} + s\mathbf{\Omega}) - f(\mathbf{x})}{s}. \tag{6.5}$$

The limit of this quotient, if it exists, is the directional derivative

$$\frac{df}{ds} = \lim_{s \to 0} \frac{f(\mathbf{x} + s\mathbf{\Omega}) - f(\mathbf{x})}{s}. \tag{6.6}$$

Because there are infinitely many directions, there are infinitely many possible directional derivatives: the rate of change of f with distance depends on direction. We might, however, suspect that directional derivatives in three orthogonal directions are sufficient to determine the directional derivative in *any* direction. To show that our suspicion is well founded, assume that f can be expanded in a Taylor series about $\mathbf{x} = (x, y, z)$:

$$f(x + s\Omega_x, y + s\Omega_y, z + s\Omega_z) = f(x, y, z) + s\Omega_x \frac{\partial f}{\partial x} + s\Omega_y \frac{\partial f}{\partial y} + s\Omega_z \frac{\partial f}{\partial z} + O(s^2), \tag{6.7}$$

where the symbol $O(s^2)$ indicates all those terms in the series in powers of 2 or greater in s. Now divide this equation by s and take the limit as s approaches zero to obtain

$$\frac{df}{ds} = \Omega_x \frac{\partial f}{\partial x} + \Omega_y \frac{\partial f}{\partial y} + \Omega_z \frac{\partial f}{\partial z}. \tag{6.8}$$

This is the scalar (or dot) product of $\mathbf{\Omega}$ with the gradient of f:

$$\frac{df}{ds} = \mathbf{\Omega} \cdot \nabla f. \tag{6.9}$$

As we suspected, to find the directional derivative in any direction, we need only the partial derivatives of f along three orthogonal axes.

6.1.2 Equation of Transfer

Once we understand the directional derivative, the equation of transfer is not difficult to derive, but we now must change our allegiance from irradiance to radiance L (Sec. 4.1.2), a function of direction specified by a unit vector $\mathbf{\Omega}$. The rate of change of L along this direction is the corresponding directional derivative $\mathbf{\Omega} \cdot \nabla L(\mathbf{\Omega})$. This rate of change is a consequence of attenuation by absorption and by scattering in all directions other than $\mathbf{\Omega}$, augmentation because of scattering into this direction from all other directions, and emission.

Attenuation of L over a distance Δs

$$\Delta L(\mathbf{\Omega}) = -L(\mathbf{\Omega})(\kappa + \beta)\Delta s \tag{6.10}$$

has the same form as attenuation of monodirectional irradiance in the two-stream theory (Sec. 5.2). And emission

$$\kappa \Delta s P_\mathrm{e}/\pi \tag{6.11}$$

has the same form as that in the two-stream theory (Sec. 5.4) with the Planck irradiance P_e replaced by the Planck radiance P_e/π. To obtain the increase in radiance along the direction Δs as a result of scattering consider Fig. 6.1, which depicts all the scatterers in a rectangular

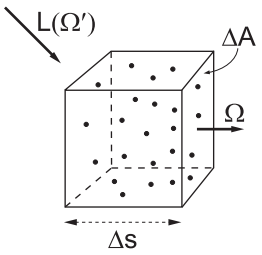

Figure 6.1: Radiation from an arbitrary direction $\mathbf{\Omega}'$ illuminating the scatterers in volume $\Delta s \Delta A$ results in scattering into a unit solid angle about the direction $\mathbf{\Omega}$ and hence contributes to the radiance in this direction.

volume $\Delta s \Delta A$ illuminated by radiation in a small solid angle $\Delta\Omega'$ about a direction $\mathbf{\Omega}'$. The associated irradiance is $L(\mathbf{\Omega}')\Delta\Omega'$, and hence the power scattered in all directions is

$$\Delta L(\mathbf{\Omega}')\Delta\Omega' N \Delta s \Delta A \sigma_{\mathrm{s}} = L(\mathbf{\Omega}')\Delta\Omega'\beta\Delta s\Delta A, \tag{6.12}$$

where the scattering coefficient β is the product of the number N of scatterers per unit volume and the scattering cross section σ_{s} per scatterer. To obtain the scattering per unit solid angle in the direction $\mathbf{\Omega}$, Eq. (6.12) must be multiplied by the probability $p(\mathbf{\Omega}', \mathbf{\Omega})$ that a photon in direction $\mathbf{\Omega}'$ is scattered into unit solid angle about the direction $\mathbf{\Omega}$. But we want the contribution to the radiance in the direction $\mathbf{\Omega}$ so must divide by the area ΔA perpendicular to this direction:

$$L(\mathbf{\Omega}')\Delta\Omega'\beta p(\mathbf{\Omega}', \mathbf{\Omega})\Delta s. \tag{6.13}$$

The contribution to the radiance in direction $\mathbf{\Omega}$ is then an integral over all directions $\mathbf{\Omega}'$:

$$\beta\Delta s \int_{4\pi} L(\mathbf{\Omega}')p(\mathbf{\Omega}', \mathbf{\Omega})\, d\mathbf{\Omega}', \tag{6.14}$$

where 4π indicates integration over all directions (4π steradians). The total change of $L(\mathbf{\Omega})$ along Δs is $\mathbf{\Omega} \cdot \nabla L(\mathbf{\Omega})\Delta s$, which when set equal to the sum of attenuation [Eq. (6.10)], emission [Eq. (6.11)], and scattering [Eq. (6.14)] yields

$$\mathbf{\Omega} \cdot \nabla L(\mathbf{\Omega}) = -(\kappa + \beta)L(\mathbf{\Omega}) + \beta \int_{4\pi} L(\mathbf{\Omega}')p(\mathbf{\Omega}', \mathbf{\Omega})\, d\mathbf{\Omega}' + \kappa P_{\mathrm{e}}/\pi. \tag{6.15}$$

L in a particular direction decreases along this direction because of absorption and scattering in all other directions, and increases because of emission and scattering into this direction. The Planck function at the temperature of the medium could vary from point to point. Emission may be negligible even if κ is not if at the wavelength of interest the Planck function is negligible. As expected, the generalization of Eq. (6.2) to an infinite number of streams yields an equation with a derivative on the left side, an integral on the right, and hence the name integro-differential equation.

From Eq. (6.15) it follows that in the absence of scattering and absorption, the radiance L along any direction is invariant (i.e., the directional derivative is zero), which we proved in

Section 4.1.3 by geometrical arguments. Pick a point in space and a direction at that point, and the radiance does not change along a line in that direction.

The probability distribution p often is called by astronomers and atmospheric scientists the *phase function*, a singularly inappropriate term given that it has nothing to do with the phases of waves but rather of astronomical bodies. We once were at a scientific meeting at which a fight almost broke out because the speaker was happily pontificating about phase functions (in the sense of angular probability distributions) while a red-faced optical scientist in the audience was excitedly hopping up and down exclaiming "but it doesn't behave that way." Order was finally restored, but it is understandable why phase function, a quantity from which phase has been removed, causes such consternation in the context of optics, a field in which the phases of waves play such a key role.

Because an incident photon becomes a scattered photon, and vice versa, if time is reversed, we must have

$$p(\mathbf{\Omega}', \mathbf{\Omega}) = p(\mathbf{\Omega}, \mathbf{\Omega}'). \tag{6.16}$$

The phase function in Eq. (6.15) is *normalized*:

$$\int_{4\pi} p(\mathbf{\Omega}, \mathbf{\Omega}')\, d\mathbf{\Omega}' = 1. \tag{6.17}$$

Other normalizations are possible so be alert for them. Equation (6.17) is a mathematical statement that if a photon is scattered it has to be scattered in *some* direction, and the set of directions in 4π steradians exhausts all of them. For an isotropic medium p cannot depend on the absolute directions $\mathbf{\Omega}'$ and $\mathbf{\Omega}$, only on the direction $\mathbf{\Omega}$ *relative* to $\mathbf{\Omega}'$, which can be expressed symbolically by writing $p(\mathbf{\Omega}' \cdot \mathbf{\Omega})$, where $\mathbf{\Omega}' \cdot \mathbf{\Omega}$ is the cosine of the angle between the two directions.

For no absorption ($\kappa = 0$) and an isotropic radiation field (L independent of direction) Eqs. (6.15) and (6.17) yield $\mathbf{\Omega} \cdot \nabla L = 0$: the radiance field is the same everywhere. This is consistent with what we obtained in Section 5.2 with the two-stream theory for a nonabsorbing medium: when the radiation field was uniform it also was isotropic.

As an aside we note that Eq. (6.15) is formally identical to the one-velocity neutron transport equation. Neutrons produced in a nuclear reactor are scattered in various directions, absorbed within it, and leak out its boundaries. The primary difference between photons and neutrons is that all photons have the same speed whereas neutrons do not. Also, neutrons, when absorbed by some nuclei, can give rise to more neutrons by way of fission reactions. But the similarities are greater than the differences, which means that mathematical techniques for solving neutron transport problems can be carried over to radiative transfer problems and vice versa.

We defined the *vector irradiance* in Section 4.2 as

$$\mathbf{F} = \int_{4\pi} \mathbf{\Omega} L(\mathbf{\Omega})\, d\mathbf{\Omega}, \tag{6.18}$$

and the *mean radiance* J is defined as

$$J = \frac{1}{4\pi} \int_{4\pi} L(\mathbf{\Omega})\, d\mathbf{\Omega}. \tag{6.19}$$

The directional derivative on the left side of Eq. (6.15) can be written

$$\mathbf{\Omega} \cdot \nabla L = \nabla \cdot (\mathbf{\Omega} L). \tag{6.20}$$

Make this substitution and integrate over all directions:

$$\int_{4\pi} \nabla \cdot (\mathbf{\Omega} L)\, d\mathbf{\Omega} = \nabla \cdot \int_{4\pi} \mathbf{\Omega} L\, d\mathbf{\Omega} = \nabla \cdot \mathbf{F}. \tag{6.21}$$

The integrated first term on the right side of the radiative transfer equation is

$$-(\kappa + \beta) \int_{4\pi} L(\mathbf{\Omega})\, d\mathbf{\Omega} = -4\pi(\kappa + \beta) J. \tag{6.22}$$

The integrated second term is

$$\beta \int_{4\pi} \int_{4\pi} p(\mathbf{\Omega}', \mathbf{\Omega}) L(\mathbf{\Omega}')\, d\mathbf{\Omega}'\, d\mathbf{\Omega}, \tag{6.23}$$

which, because of the normalization condition Eq. (6.17), is

$$\beta \int_{4\pi} L(\mathbf{\Omega}')\, d\mathbf{\Omega}' = 4\pi\beta J. \tag{6.24}$$

The integrated third term is $4\kappa P_{\mathrm{e}}$, which when combined with Eqs. (6.21), (6.22) and (6.24) yields

$$\nabla \cdot \mathbf{F} = -4\pi\kappa J + 4\kappa P_{\mathrm{e}}. \tag{6.25}$$

This is a general result, as valid as the equation of transfer. And it makes physical sense. For a nonabsorbing medium ($\kappa = 0$) the divergence of the vector irradiance is zero: all the photons that enter a region come out.

To explain briefly why Eq. (6.15) can lead to such a bewildering array of N-stream approximations we back up just a bit. Consider first approximating an arbitrary one-dimensional integral as a finite sum:

$$\int_a^b f(x)\, dx \approx \sum_{j=1}^{N} w_j f(x_j). \tag{6.26}$$

This is called reducing an integral to *quadratures*; the w_j are quadrature weights and the discrete set of ordinates x_j are quadrature points. Simpson's rule, which you may remember from elementary calculus, is a quadrature formula, one of the simplest imaginable. Note the tremendous latitude of choices with which we are faced: N, w_j, and x_j, a triply-infinite set of possibilities. Thus there are many ways of replacing the integro-differential equation Eq. (6.15) with a set of N coupled ordinary differential equations for L in N discrete directions depending on the many ways of approximating the integral on the right side by a finite sum. This approach goes under the general name of *discrete ordinates*.

At this point, however, we are not going to launch into discussing the many ways of obtaining approximate solutions to Eq. (6.15). There are many methods and countless variations on them, most of them restricted to plane-parallel media (which don't exist). To learn more about all these methods consult the references at the end of this chapter. Instead of discussing even a restricted set of such methods, we devote Section 6.3 to only one, the Monte Carlo method, which has the peculiar characteristic that it enables us to solve equations even if we don't know what they are. By Monte Carlo methods, which are not restricted to plane-parallel media, one can solve Eq. (6.15) without knowing that it exists. Sound like magic? Read on.

6.2 Diffusion Theory: The Elements

Equation (6.25) doesn't do us much good because it contains two unknown quantities, and so we have to go a step further and make some approximations. The quantity J at a point, which we take to be a spectral quantity (i.e., we consider only photons with a narrow range of energies), is, except for a multiplicative factor, the number density of photons. That is, L is the number density of photons moving in a given direction per unit solid angle times the speed of a photon times the photon energy. When we integrate this quantity over all directions we get the total number of photons per unit volume. According to molecular diffusion theory, transport is driven by concentration gradients (Fick's law). The same must be true for photons, so we postulate a diffusion law for photons:

$$\mathbf{F} = -4\pi D \nabla J, \tag{6.27}$$

where D is the photon *diffusion coefficient*, here assumed independent of position, and the factor 4π is introduced for convenience. Now combine Eqs. (6.25) and (6.27) to obtain the diffusion equation

$$\nabla^2 J - \frac{1}{\chi^2} J = 0, \tag{6.28}$$

where the *diffusion length* χ is

$$\chi^2 = \frac{D}{\kappa}. \tag{6.29}$$

We have an equation for the mean radiance J but what about the radiance L? The radiance distribution

$$L = J - 3D\boldsymbol{\Omega} \cdot \nabla J \tag{6.30}$$

is consistent with Eq. (6.27), Fick's law for photons. To show this, multiply both sides of Eq. (6.30) by $\boldsymbol{\Omega}$ and integrate over all directions:

$$\int_{4\pi} L\boldsymbol{\Omega}\, d\boldsymbol{\Omega} = \mathbf{F} = \int_{4\pi} \boldsymbol{\Omega} J\, d\boldsymbol{\Omega} - 3D \int_{4\pi} \boldsymbol{\Omega}(\boldsymbol{\Omega} \cdot \nabla J)\, d\boldsymbol{\Omega}. \tag{6.31}$$

The first integral on the right side vanishes; the second, after a bit of effort, can be shown to be $4\pi\nabla J/3$, which when substituted in Eq. (6.31) yields Eq. (6.27). Thus diffusion theory

is based on the assumption that the radiance is a linear function of direction relative to the gradient of the mean radiance.

All that is left is to determine the diffusion coefficient. Multiply both sides of Eq. (6.15) by $\mathbf{\Omega}$, assume there is negligible emission and integrate over all directions:

$$\int_{4\pi} \mathbf{\Omega}(\mathbf{\Omega}\cdot\nabla L)\, d\mathbf{\Omega} = -(\kappa+\beta)\int_{4\pi} \mathbf{\Omega} L\, d\mathbf{\Omega} + \beta\int_{4\pi}\int_{4\pi} p(\mathbf{\Omega}', \mathbf{\Omega})\mathbf{\Omega} L(\mathbf{\Omega}')\, d\mathbf{\Omega}'\, d\mathbf{\Omega}. \quad (6.32)$$

The first integral on the right side of Eq. (6.32) is the vector irradiance [Eq. (6.18)]. The second integral is a double integral, which we can integrate sequentially. Consider first the integral

$$\int_{4\pi} p(\mathbf{\Omega}', \mathbf{\Omega})\mathbf{\Omega}\, d\mathbf{\Omega}. \quad (6.33)$$

This integral is a vector, call it $\mathbf{G}$, and take its dot product with $\mathbf{\Omega}'$:

$$\int_{4\pi} p(\mathbf{\Omega}', \mathbf{\Omega})\mathbf{\Omega}'\cdot\mathbf{\Omega}\, d\mathbf{\Omega} = \mathbf{\Omega}'\cdot\mathbf{G}. \quad (6.34)$$

The integral on the left side of Eq. (6.34) is the asymmetry parameter g, the mean cosine of the scattering angle:

$$g = \mathbf{\Omega}'\cdot\mathbf{G}. \quad (6.35)$$

If the medium is isotropic, g does not depend on $\mathbf{\Omega}'$, which implies that Eq. (6.33) is

$$G = g\mathbf{\Omega}'. \quad (6.36)$$

Substitute this result in Eq. (6.32) to obtain

$$\int_{4\pi} \mathbf{\Omega}(\mathbf{\Omega}\cdot\nabla L)\, d\mathbf{\Omega} = -\{\beta(1-g)+\kappa\}\mathbf{F}. \quad (6.37)$$

This result is quite general. To go further we have to make some approximations. For L in Eq. (6.37) take Eq. (6.30); the result for the left side of Eq. (6.37) is

$$\int_{4\pi} \mathbf{\Omega}(\mathbf{\Omega}\cdot\nabla J)\, d\mathbf{\Omega} - 3D\int_{4\pi} \mathbf{\Omega}\{\mathbf{\Omega}\cdot\nabla(\mathbf{\Omega}\cdot\nabla J)\}\, d\mathbf{\Omega}. \quad (6.38)$$

The first integral was obtained previously in the derivation of Eq. (6.31). The second integral, with much labor, can be shown to vanish. Thus we have

$$\mathbf{F} = -\frac{4\pi}{3\{\beta(1-g)+\kappa\}}\nabla J, \quad (6.39)$$

which from Eq. (6.27) gives the diffusion coefficient

$$D = \frac{1}{3\{\beta(1-g)+\kappa\}}. \quad (6.40)$$

This is consistent with the two-stream theory for an absorbing medium. We obtained a diffusion equation (one-dimensional) [Eq. (5.69)] identical to Eq. (6.28), satisfied by both upward and downward irradiances. From that result we can infer a diffusion coefficient given by Eq. (6.40) but without the factor 3.

The diffusion equation for the mean radiance [Eq. (6.28)] and the diffusion coefficient [Eq. (6.40)] are not sufficient by themselves. We also need boundary conditions. These are based on irradiances. Consider a surface the normal to which is the unit vector $\mathbf{n}$. The irradiance associated with this surface is

$$\int_{2\pi} L\,\mathbf{n}\cdot\mathbf{\Omega}\,d\mathbf{\Omega} = F, \tag{6.41}$$

where 2π indicates integration over a hemisphere of directions centered on $\mathbf{n}$. Substitute Eq. (6.30) in Eq. (6.41) to obtain

$$F = J\mathbf{n}\cdot\int_{2\pi}\mathbf{\Omega}\,d\mathbf{\Omega} - 3D\mathbf{n}\cdot\int_{2\pi}\mathbf{\Omega}(\mathbf{\Omega}\cdot\nabla J)\,d\mathbf{\Omega}. \tag{6.42}$$

The first integral is π; the second integral is similar to the second integral on the right side of Eq. (6.33). We therefore obtain

$$F = \pi J - 2\pi D\mathbf{n}\cdot\nabla J. \tag{6.43}$$

With this equation we can impose various conditions on the irradiance at boundaries. With Eqs. (6.28) and (6.43) in hand, together with the diffusion coefficient Eq. (6.40), we now can take advantage of the huge literature on solutions to diffusion equations for various geometries and boundary conditions. Given the similarity between diffusion theory and the two-stream theory for an absorbing medium, we expect the two approximations to have the same degree of applicability. The difference is that the diffusion equation [Eq. (6.28)] allows us to solve problems for other than plane-parallel media.

Without solving the diffusion equation we can use it to gain some insight into when vertical attenuation within a laterally finite absorbing medium is dominated by its intrinsic properties (i.e., its diffusion length) rather than by leakage out its sides. Because of the form of the diffusion equation [Eq. (6.28)] we expect attenuation along a vertical line to be determined mostly by the diffusion length if the line is a few diffusion lengths from the lateral boundaries. Within a diffusion length or less, attenuation is more and more determined by leakage out the boundaries.

If the single-scattering albedo is close to 1, as it is for clouds at visible wavelengths, the diffusion length [Eq. (6.29)] is

$$\chi \approx \frac{1}{\beta\sqrt{3(1-\omega)(1-g)}}. \tag{6.44}$$

If we approximate β as $3f/d$, where f is the volume fraction of cloud droplets and d is the droplet diameter, we obtain

$$\chi \approx \frac{d}{f\sqrt{3(1-g)(1-\varpi)}}. \tag{6.45}$$

For cloud droplets g is around 0.85, and so we can take the square root of $3(1-g)$ to be 1. The volume fraction f is around 10^{-6} or less and d is of order 10 μm, which yields

$$\chi \approx \frac{10}{\sqrt{1-\varpi}} \tag{6.46}$$

for the diffusion length in meters. If $\varpi = 0.9999$, the diffusion length is 1 km; if $\varpi = 0.999999$, the diffusion length is 10 km. Thus if we wished to determine the diffusion length of a cloud by measuring attenuation within it, we would have to do so along a line a few kilometers from its lateral boundaries.

6.3 The Monte Carlo Method

In the Monte Carlo method applied to radiative transfer, photons are treated statistically. The distance a photon travels before something happens to it (scattering or absorption) is given by a probability distribution. Having traveled this distance it has a specified probability of being either absorbed or scattered. If scattered, the direction of scattering is determined by another probability distribution. One after another photons are imagined to be launched into a medium. As with humans, "time and chance happeneth to them all." The ultimate fate of a photon is either capture by the medium (absorption) or escape from it. Enough photon histories are accumulated to give a statistically valid picture of reflection, transmission, and absorption by a medium illuminated by greatly many photons. The heart of the Monte Carlo method is transforming from probability distributions for physical variables to a uniform probability distribution. Everything else is bookkeeping.

Suppose that we have a probability distribution $p(x)$ for a variable x. Recall that probability distributions are defined by their integral values in that

$$\int_{x_1}^{x_2} p(x)\, dx \tag{6.47}$$

is the probability that x lies in the interval between x_1 and x_2. The integral of p over all x is 1. We want to transform to a variable ξ the values of which are *uniformly* distributed between 0 and 1. That is, ξ is a random number with probability distribution $P(\xi) = 1$. We want to find x as a function of ξ such that we obtain p. From the theorem for transforming variables of integration we have

$$\int_{\xi_1}^{\xi_2} p(x)\frac{dx}{d\xi}\, d\xi = \int_{\xi_1}^{\xi_2} P(\xi)\, d\xi. \tag{6.48}$$

For this always to be true requires that the integrands be equal:

$$p(x)\frac{dx}{d\xi} = P(\xi) = 1. \tag{6.49}$$

This is a first-order differential equation for x as a function of ξ. If we can solve it, we should be able to recover the probability distribution $p(x)$ as follows.

Divide the x-axis into a large set of intervals (or bins). The j^{th} bin is defined by those values lying between x_j and x_{j+1}. Choose a value of ξ randomly and find the corresponding value of x. Assign this value to a bin. After doing this a great many times, divide the number in each bin by the total number of values. This gives the probabilities of x lying in each bin. Divide by the bin width to obtain the probability density. Now plot these probability densities versus x. In the limit of an indefinitely large number of bins and random numbers ξ this result should converge to the probability distribution $p(x)$.

To show that it does consider a simple linear probability distribution $p = 2x$ on the interval $0 \leq x \leq 1$. As required, the integral of p over this interval is 1. The differential equation for the transformation is

$$2x\frac{dx}{d\xi} = \frac{d}{d\xi}\left(x^2\right) = 1, \tag{6.50}$$

the solution to which, subject to the boundary condition $x = 0$ when $\xi = 0$, is

$$x = \sqrt{\xi}. \tag{6.51}$$

Figure 6.2 shows the results of using a random number generator to compute N values of ξ and the corresponding values of x in 100 bins. The computed probability density is shown as dots. As N increases, the dots lie more closely to the exact probability distribution. If for fixed N the same set of calculations is done again and again the distribution of dots will not be exactly the same. This is shown in Fig. 6.3 for 100 bins and two sets of 10^6 random numbers.

The previous paragraphs are general. Now we have to get specific in order to develop a computational method in detail. For this we need probability distributions for path lengths and scattering directions, which we turn to next.

6.3.1 Path Length Distribution

The probability distribution for the path length x a photon travels before it is scattered or absorbed is given in Section 5.1, rewritten here as

$$p(x) = \frac{1}{\ell}\exp(-x/\ell), \tag{6.52}$$

where x is the *physical* path length and ℓ the total mean free path. It is more convenient here to express this distribution in terms of the *optical* path length $\tau = x/\ell$:

$$p(\tau) = \exp(-\tau), \tag{6.53}$$

the integral of which from 0 to ∞ is 1, as it must be if this is a proper probability distribution. As we did previously for the probability distribution $2x$, we find τ as a function of ξ, a random number between 0 and 1 with a uniform probability distribution, such that

$$p(\tau)\frac{d\tau}{d\xi} = -\frac{d}{d\xi}\exp(-\tau) = P(\xi) = 1. \tag{6.54}$$

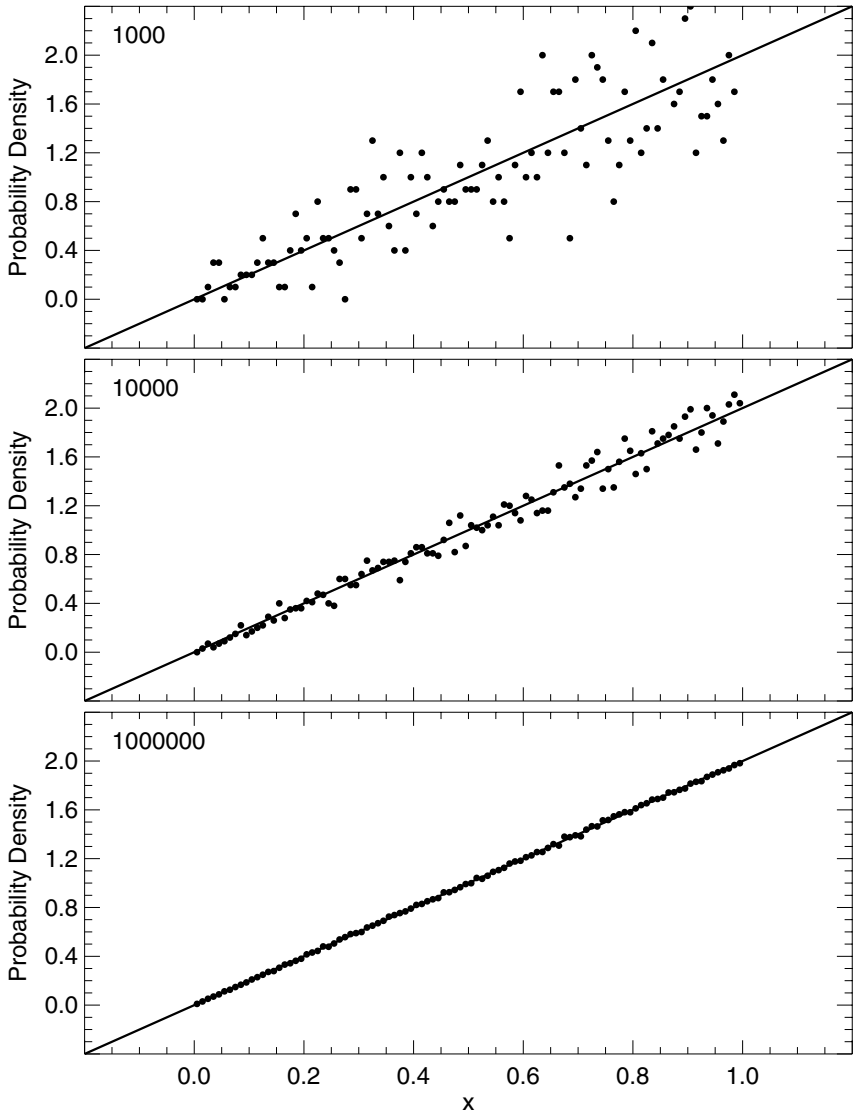

Figure 6.2: The continuous probability distribution $p = 2x$ (solid curve) for the variable x can be approximated by dividing the x-axis into equal intervals (bins); 100 bins were used here. Values are assigned to each bin with a random number generator. The number of values in each bin divided by the total number is the probability of a value lying within a bin. Divide by the bin width to obtain the probability density. The discrete probability densities more closely approximate the continuous distribution the greater the number of values (indicated in the upper left corner of each plot).

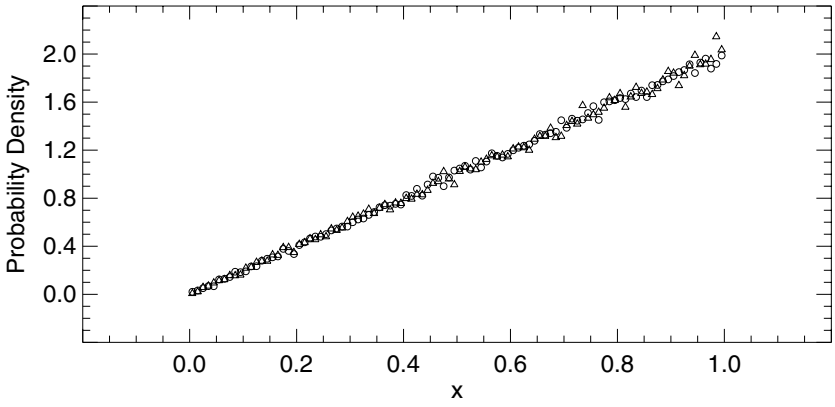

Figure 6.3: The same calculations shown in Fig. 6.2 for 1000000 random numbers but done two times. The probability densities for each run are shown with open circles and open triangles.

The solution to this differential equation, subject to the boundary condition $\tau = 0$ when $\xi = 1$, is

$$\tau = -\ln(1 - \xi). \tag{6.55}$$

With this transformation, the random number ξ is uniformly distributed between 0 and 1 and the optical path length τ is distributed between 0 and ∞ according to the probability distribution Eq. (6.53).

To show this the τ-axis was divided into bins of width 0.01, 10^6 random numbers ξ chosen, the corresponding values of τ calculated from Eq. (6.55) and assigned to appropriate bins, and the fraction of values in each bin divided by the bin width 0.01 and plotted. As expected, this set of discrete probability densities (Fig. 6.4) lies close to the continuous probability distribution $\exp(-\tau)$.

Given that a photon travels an optical path τ before something happens to it, the probability it is scattered is the single-scattering albedo ϖ, and hence the probability it is absorbed is $1 - \varpi$. Thus to determine if a photon is scattered or absorbed, compute a random number. If it is less than or equal to ϖ, the photon is scattered; if not, the photon is absorbed, its death duly recorded, another photon launched, and so on into the long hours of night. If a photon is scattered, the direction of its next path is determined by a probability distribution for scattering directions.

6.3.2 Scattering Direction Distribution

The probability distribution for scattering in a particular direction per unit solid angle is specified by the inaptly-named phase function $p(\vartheta, \varphi)$ (see Sec. 6.1.2), normalized in that

$$\int_0^{2\pi} \int_0^{\pi} p(\vartheta, \varphi) \sin\vartheta \; d\vartheta \; d\varphi = 1, \tag{6.56}$$

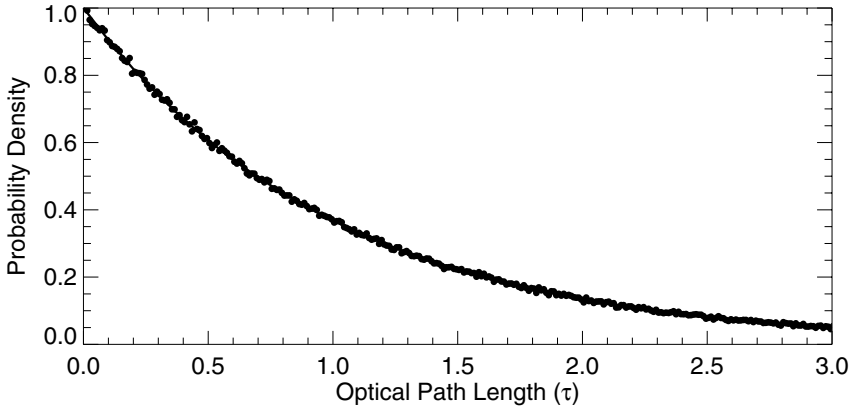

Figure 6.4: The continuous probability distribution $p = \exp(-\tau)$ for the variable τ can be approximated by dividing the τ-axis into equal intervals (bins); 1000 bins were used here. Values are assigned to each bin with a random number generator. The number of values in each bin divided by the total number times the bin width is the probability density for the bin. The discrete probability densities (solid circles) more closely approximate the continuous distribution (solid line) the greater the number of random numbers.

where the z-axis for the spherical polar coordinate system (ϑ, φ) is the direction a photon had *before* it was scattered, ϑ is the scattering angle and φ the azimuthal angle. More often than not, scattering is taken to be azimuthally symmetric (i.e., p is independent of φ), which implies that all azimuthal angles are equally probable, and hence the phase function can be written

$$p(\vartheta, \varphi) = \frac{p(\vartheta)}{2\pi}, \tag{6.57}$$

where $1/2\pi$ is the (uniform) probability distribution for azimuthal angles. By transforming to the variable $\mu = \cos\vartheta$, the normalization condition Eq. (6.56) becomes

$$\int_{-1}^{1} p(\mu)\, d\mu = 1. \tag{6.58}$$

Azimuthal symmetry is strictly valid only for a spherically symmetric medium (i.e., one that doesn't change if it is rotated) and for radiation that is unpolarized.

Determining the azimuthal angle for a scattered photon is straightforward: generate a random number ξ between 0 and 1, and the azimuthal angle is $2\pi\xi$. What about the scattering angle? If the scatterers are spheres, we can calculate $p(\mu)$ from Mie theory. If they are not spheres, recourse may be had to other theories or even measurements. What is often done, however, is to use the simple one-parameter *Henyey–Greenstein* phase function

$$p(\mu) = \frac{1}{2}\frac{1 - g^2}{(1 + g^2 - 2g\mu)^{3/2}}. \tag{6.59}$$

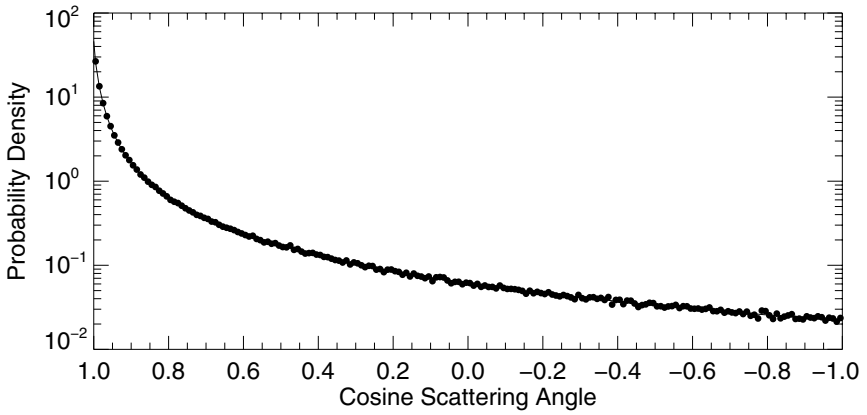

Figure 6.5: Henyey–Greenstein angular scattering probability distribution (solid curve) approximated by discrete probability densities (solid circles) obtained by dividing the range of cosines into equal intervals (bins), assigning values to each bin randomly, and dividing the fraction of values in a bin by its width. The asymmetry parameter is 0.85.

We emphasize that this phase function has no physical significance whatsoever. It is a mathematical phase function that bears some resemblance to physical phase functions and has a few desirable mathematical properties. For example, it is normalized, which is no trick given that *any* function can be normalized. More important, g (asymmetry parameter) in Eq. (6.59) is the mean cosine of the scattering angle:

$$\langle \mu \rangle = \int_{-1}^{1} \mu p(\mu)\, d\mu = g. \tag{6.60}$$

In the limit $g \to 1$, p is an infinite spike in the forward direction ($\mu = 1$), whereas in the limit $g \to -1$, p is an infinite spike in the backward direction ($\mu = -1$). That is,

$$\lim_{g\to 1} p(1) = \lim_{g\to 1} \frac{1+g}{(1-g^2)} = \infty,\ p(\mu < 1,\ g = 1) = 0, \tag{6.61}$$

$$\lim_{g\to -1} p(-1) = \lim_{g\to -1} \frac{1-g}{(1+g^2)} = \infty,\ p(-1 < \mu,\ g = -1) = 0. \tag{6.62}$$

For $g = 0$, the Henyey–Greenstein function corresponds to isotropic scattering, which, as we note in Section 5.2 (and explain in Sec. 7.3), does not exist for electromagnetic radiation.

As we did with the probability distribution for photon path lengths, we need to find the transformation to the random variable ξ by way of a first-order differential equation:

$$p(\mu)\frac{d\mu}{d\xi} = \frac{1-g^2}{2g}\frac{d}{d\xi}\frac{1}{(1+g^2-2g\mu)^{1/2}} = 1, \tag{6.63}$$

the solution to which, subject to the boundary condition $\mu = -1$ when $\xi = 0$, is

$$\mu = \frac{1}{2g}\left\{1 + g^2 - \left(\frac{1 - g^2}{1 - g + 2g\xi}\right)^2\right\}. \tag{6.64}$$

The μ-axis was divided into bins of width 0.01, 10^6 random numbers ξ chosen, the corresponding values of μ calculated from Eq. (6.64) for $g = 0.85$ and assigned to appropriate bins, and the fraction of values in each bin divided by the bin width and plotted. As expected, this set of discrete probability densities (Fig. 6.5) lies close to the continuous probability distribution [Eq. (6.59)].

Given the shaky theoretical foundation for the Henyey–Greenstein phase function, how does it compare with one more firmly supported? Figure 6.6 compares the Henyey–Greenstein phase function with calculations using Mie theory for a lognormal distribution of cloud droplets. Agreement is good except close to the forward direction and for scattering angles greater than about $120°$. Scattering is much less in these backward directions, however, so the disagreement, although relatively large, more than a factor of 10, is absolutely small. If one were interested in backscattering by an optically thin medium ($\tau \ll 1$), the Henyey–Greenstein function would be inappropriate. For an optically thick medium ($\tau \gg 1$), multiple scattering effaces almost all details of the phase function except the mean cosine of the scattering angle. Less important than the correctness of *each* scattering event is the correctness of the average over *many* events. A corollary of this is that the Henyey–Greenstein phase function is likely to be at its worst for calculations of reflection by media with optical thicknesses around 1.

The sharp rise of the theoretical phase function near the forward direction is almost 100 times greater than the Henyey–Greenstein phase function. But what appears to be a weakness is actually a strength. A narrow peak near the forward direction corresponds to almost no scattering in the sense that photons are hardly diverted from their original direction. This suggests that pesky near-forward scattered photons can be whisked out of sight as follows. Approximate the product of the scattering coefficient β and theoretical phase function $\tilde{p}$ (e.g., from Mie theory) as the weighted sum of a Henyey–Greenstein phase function $\overline{p}$ with asymmetry parameter $\overline{g}$ and an infinitely sharp spike in the forward direction:

$$\beta\tilde{p} \approx \overline{\beta}\overline{p} + \beta_0\delta, \tag{6.65}$$

where

$$\delta(\mu) = \lim_{g\to 1} p(\mu), \tag{6.66}$$

and both p and $\overline{p}$ are given by Eq. (6.59). Because $\tilde{p}$, $\overline{p}$, and δ are normalized

$$\beta \approx \overline{\beta} + \beta_0. \tag{6.67}$$

The asymmetry parameter is

$$g = \int_{-1}^{1} \mu\tilde{p}\, d\mu = \frac{\overline{\beta}}{\beta}\overline{g} + \frac{\beta_0}{\beta}. \tag{6.68}$$

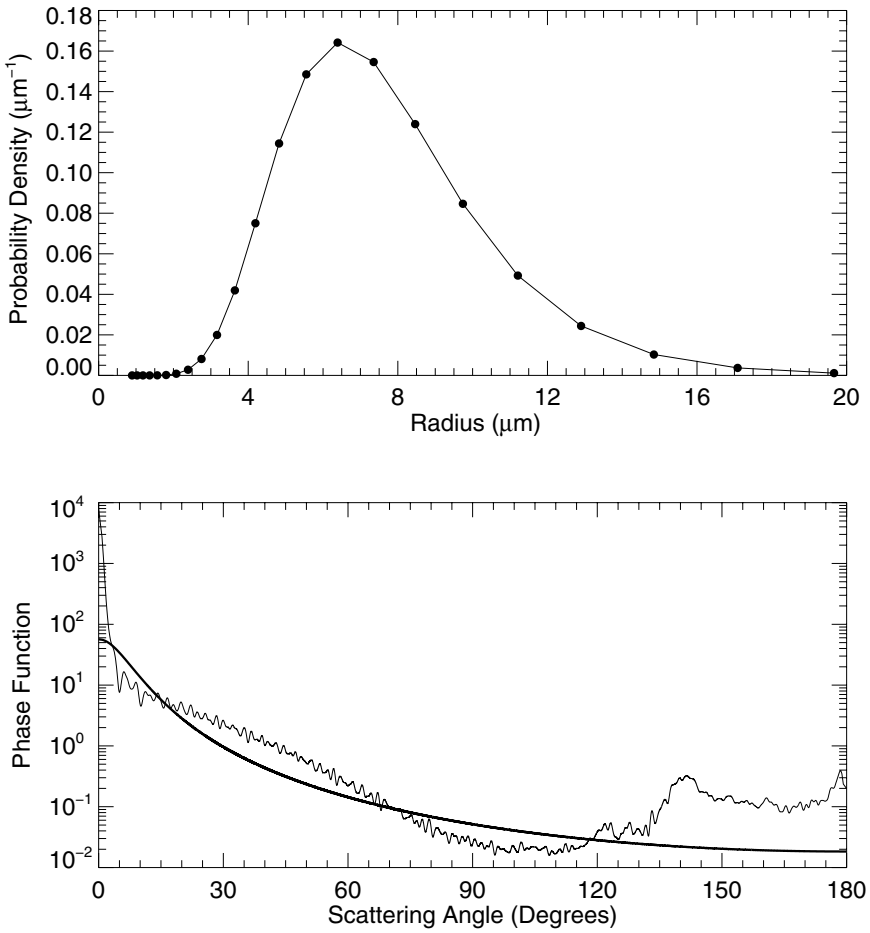

Figure 6.6: Lognormal size distribution of cloud droplets (top panel) for the phase function calculated with Mie theory (thin line) in the bottom panel compared with the Henyey–Greenstein phase function (thick line) with $g = 0.87$, also calculated with Mie theory. The wavelength of the illumination is 550 nm.

From Eqs. (6.67) and (6.68) it therefore follows that a real medium with scattering coefficient β and asymmetry parameter g is approximately equivalent to a fictitious medium with scattering coefficient

$$\overline{\beta} = \beta - \beta_0 \tag{6.69}$$

and a Henyey–Greenstein phase function with asymmetry parameter given by

$$\overline{g} = 1 - \frac{\beta}{\overline{\beta}}(1-g) \tag{6.70}$$

provided that scattering by the medium is highly peaked near the forward direction (i.e., the scatterers are large compared with the wavelength). Now we have to choose the ratio $\beta/\overline{\beta}$. For example, we argued in Section 3.5.2 that in the limit of infinite radius, half of the scattering cross section of a sphere is associated with scattering in the forward direction, and hence for a sufficiently large sphere $\beta/\overline{\beta} \approx 2$. With this approximation the scattering coefficient of the fictitious medium is $\beta/2$ and its asymmetry parameter is $1 - 2(1-g)$.

6.3.3 Transforming Coordinate Axes

The trajectory of a photon is a sum of vectors $\tau_1\mathbf{\Omega}_1$, $\tau_2\mathbf{\Omega}_2$, ..., where τ_j are optical path lengths and $\mathbf{\Omega}_j$ are unit vectors. In previous sections we showed how to generate τ_j and $\mathbf{\Omega}_j$. The catch is that each direction vector $\mathbf{\Omega}_j$ is specified by a scattering angle ϑ_j and azimuthal angle φ_j relative to a *different* coordinate system. Thus to add these vectors we have to transform them all to a common (reference) coordinate system. How this is done for two successive directions sets the pattern for an arbitrary number of directions.

The first direction vector of a photon launched into a medium is

$$\mathbf{\Omega}_1 = \sin\vartheta_1\cos\varphi_1\mathbf{i}_1 + \sin\vartheta_1\sin\varphi_1\mathbf{j}_1 + \cos\vartheta_1\mathbf{k}_1, \tag{6.71}$$

where $\mathbf{i}_1, \mathbf{j}_1, \mathbf{k}_1$ are unit vectors along the coordinate axes of the reference coordinate system. For the second direction we define a new coordinate system with

$$\mathbf{k}_2 = \mathbf{\Omega}_1. \tag{6.72}$$

The three vectors $\mathbf{i}_2, \mathbf{j}_2, \mathbf{k}_2$, where

$$\mathbf{i}_2 = \cos\vartheta_1\cos\varphi_1\mathbf{i}_1 + \sin\vartheta_1\sin\varphi_1\mathbf{j}_1 + \cos\vartheta_1\mathbf{k}_1, \tag{6.73}$$

$$\mathbf{j}_2 = -\sin\varphi_1\mathbf{i}_1 + \cos\varphi_1\mathbf{j}_1, \tag{6.74}$$

form an orthonormal, right-handed system. That is, they are of unit length, mutually perpendicular and

$$\mathbf{i}_2 \times \mathbf{j}_2 = \mathbf{k}_2,\ \mathbf{k}_2 \times \mathbf{i}_2 = \mathbf{j}_2,\ \mathbf{j}_2 \times \mathbf{k}_2 = \mathbf{i}_2. \tag{6.75}$$

Equations (6.72)–(6.74) can be written in matrix form

$$\begin{pmatrix} \mathbf{i}_2 \\ \mathbf{j}_2 \\ \mathbf{k}_2 \end{pmatrix} = \begin{pmatrix} \cos\vartheta_1\cos\varphi_1 & \cos\vartheta_1\sin\varphi_1 & -\sin\vartheta_1 \\ -\sin\varphi_1 & \cos\varphi_1 & 0 \\ \sin\vartheta_1\cos\varphi_1 & \sin\vartheta_1\sin\varphi_1 & \cos\vartheta_1 \end{pmatrix} \begin{pmatrix} \mathbf{i}_1 \\ \mathbf{j}_1 \\ \mathbf{k}_1 \end{pmatrix}. \tag{6.76}$$

The second direction is specified by the unit vector

$$\mathbf{\Omega}_2 = \sin\vartheta_2\cos\varphi_2\mathbf{i}_2 + \sin\vartheta_2\sin\varphi_2\mathbf{j}_2 + \cos\vartheta_2\mathbf{k}_2, \tag{6.77}$$

where ϑ_2 is the scattering angle and φ_2 the azimuthal angle. Given Eqs. (6.76) and (6.77), we can express $\mathbf{\Omega}_2$ relative to the reference coordinate system. For the next scattering direction $\mathbf{\Omega}_3$, the unit vectors in the local coordinate system are given by Eq. (6.76) with 2 replaced by 3, 1 replaced by 2. The components of this direction in the reference coordinate system are obtained by multiplying two matrices. For the next direction, multiply three matrices, and so on. We can write this compactly in matrix notation:

$$\boldsymbol{\xi}_n = \mathbf{M}_{n-1}\mathbf{M}_{n-2}\ldots\mathbf{M}_1\boldsymbol{\xi}_1, \tag{6.78}$$

where

$$\boldsymbol{\xi}_p = \begin{pmatrix} \mathbf{i}_p \\ \mathbf{j}_p \\ \mathbf{k}_p \end{pmatrix}, \ \mathbf{M}_p = \begin{pmatrix} \cos\vartheta_p\cos\varphi_p & \cos\vartheta_p\sin\varphi_p & -\sin\vartheta_p \\ -\sin\varphi_p & \cos\varphi_p & 0 \\ \sin\vartheta_p\cos\varphi_p & \sin\vartheta_p\sin\varphi_p & \cos\vartheta_p \end{pmatrix}. \tag{6.79}$$

6.3.4 Surface Reflection

The results so far enable us to determine the statistical behavior of photons *within* a medium: probabilities of distances traveled before an event (scattering or absorption), if the event is scattering or absorption, and, if scattering, the probability of a particular scattering direction. But what happens when a photon encounters a *boundary*? This depends on its reflecting properties. If the reflectivity is zero, the photon is counted as having been removed from the medium. But for a nonzero reflectivity, the photon has a nonzero probability of being reflected back into the medium. Moreover, this probability could depend on the direction of incidence of the photon, and the direction of reflection specified by a different probability distribution for each incident direction.

The simplest idealized reflecting boundary is *diffuse*: the probability distribution for reflected photons is independent of the direction of incidence and the reflected radiation is isotropic. With these assumptions the probability distribution for reflection directions is

$$p(\vartheta,\varphi) = \frac{\cos\vartheta\sin\vartheta}{\pi}, \tag{6.80}$$

where ϑ is the angle between the normal to the reflecting boundary and the reflection direction and φ is its azimuthal angle. The factor π ensures that p is normalized:

$$\int_0^{2\pi}\int_0^{\pi/2} p(\vartheta,\varphi)\, d\vartheta\, d\varphi = 1. \tag{6.81}$$

If a (albedo or reflectivity) is the probability that an incident photon is reflected, to determine if a photon is absorbed at a boundary choose a random number ξ between 0 and 1. If $\xi > a$, the photon is absorbed. If not absorbed, it is reflected, and it follows from Eqs. (6.49) and (6.80) that the distribution of reflected azimuthal angles is specified by

$$\varphi = 2\pi\xi \tag{6.82}$$

and of co-latitudes by

$$\vartheta = \sin^{-1}\left(\sqrt{\xi}\right). \tag{6.83}$$

6.3.5 Emission

As noted in Section 6.1.2, emission may be negligible at a particular wavelength even though absorption is not because of the Planck function multiplying the absorption coefficient in the equation of transfer [Eq. (6.15)]. This function depends on temperature. For terrestrial temperatures emission at visible and near-visible wavelengths is exceedingly small, and so the Planck function can be neglected. But if scattering is negligible whereas emission is not, the equation of transfer becomes a first-order differential equation

$$\mathbf{\Omega} \cdot \nabla L(\mathbf{\Omega}) = -\kappa L(\mathbf{\Omega}) + \kappa P_{\mathrm{e}}/\pi. \tag{6.84}$$

The term on the left is a directional derivative, the rate of change of L with respect to distance s along each direction, and so we can write this equation as

$$\frac{dL}{ds} = -\kappa L + \kappa P_{\mathrm{e}}/\pi. \tag{6.85}$$

If we transform the independent variable from physical distance s to absorption optical thickness along a given path

$$\tau = \int_0^s \kappa(s')\, ds', \tag{6.86}$$

Eq. (6.85) becomes

$$\frac{dL}{d\tau} = -L + P_{\mathrm{e}}/\pi, \tag{6.87}$$

the solution to which is

$$L(\tau) = L_0 \exp(-\tau) + \frac{1}{\pi} \int_0^\tau \exp\{-(\tau - \tau')\} P_{\mathrm{e}}(\tau')\, d\tau'. \tag{6.88}$$

The interpretation of this equation is straightforward: the first term is the contribution to the total radiance by attenuation of a known radiance at some reference point (which could be at a boundary); the second term is the contribution from radiation emitted at every point of a path and attenuated from the emission point to the point of interest. Note the similarity between this equation and the two-stream equations for emission in Section 5.4. Keep in mind that L and P_{e} depend on absorption optical thickness along a path in a given direction between two points in the medium. This dependence is, in general, different for every path and may be quite complicated for heterogeneous media. But in principle we can find the radiance in any direction at any point in the medium by integration along a path in that direction beginning at a point where the radiance is known.

But suppose that we want the *irradiance* F. From the point of interest extrapolate backwards on a straight line to a point where the radiance is known and calculate the radiance with Eq. (6.88). This is for only one direction. To estimate the irradiance requires sampling a sufficient number of directions that the quadrature

$$F = \int_{2\pi} L(\mathbf{\Omega})\, \mathbf{n} \cdot \mathbf{\Omega}\, d\mathbf{\Omega} \approx \sum_i \sum_j w_{ij} L(\vartheta_j, \varphi_i), \tag{6.89}$$

is accurate, where (ϑ_j, φ_i) specifies a direction relative to the normal $\mathbf{n}$ to a plane at the point of interest and the w_{ij} are quadrature weights.

The Planck function in Eq. (6.88) depends on the absolute temperature along the integration path. In Earth's atmosphere, temperature usually decreases with height in the troposphere, although the fractional change in absolute temperature is only about 20%. But because of the strong dependence of emission on absolute temperature (see Sec. 1.2.2), the vertical variation of temperature cannot be neglected.

Scattering of terrestrial radiation by clear air usually is negligible. For example, scattering at $10\,\mu\mathrm{m}$ is about 10^4 times smaller than at $1\,\mu\mathrm{m}$, and hence Eq. (6.88) is applicable to clear air. Scattering of terrestrial radiation by clouds, although often neglected, is not obviously negligible, as evidenced by the single-scattering albedo of a cloud droplet for such radiation (Fig. 5.15). Equation (6.88) is also applicable to a cloudy atmosphere for which scattering is negligible. Any of the methods for solving the plane-parallel radiative transfer equation can be used for a cloudy atmosphere in which neither scattering nor emission are negligible. So this leaves us with only one kind of emitting and scattering medium – vertically and horizontally inhomogeneous – to address. How do we tackle such a medium with the Monte Carlo method?

To answer this question, first consider a negligibly scattering medium (which can be treated by other methods). Divide this medium into small volumes (boxes). The key step is determining emission in many directions for each box. Pick points on the faces of a box at random, and for each point A choose an outward direction at random. Trace a ray in this direction backwards from A until it exits the box at point B. Calculate the radiance emerging at A by evaluating the integral in Eq. (6.88) along the path BA. Do this for enough points and directions to obtain a good estimate of the radiation emitted by each box. The result is a finite set of sources distributed throughout the medium, the radiation from which can be treated as in previous Monte Carlo calculations. This approach was used to calculate the upward and downward clear-sky terrestrial irradiances shown in Fig. 6.20, which are indistinguishable from irradiances obtained from a solution to the plane-parallel equation.

What if a box contains scatterers? The backwards approach still is used, but because of scattering within a box, a bundle follows a zig-zag path from A to B. As with a negligibly scattering box, the contribution to the source is obtained by integration of Eq. (6.88) along this path. Again, the end result is a set of boxes, each a source of radiation to which the usual Monte Carlo method is applied.

Although this scheme for radiative transfer in emitting and scattering media can be described simply and briefly, writing computer programs to obtain numbers requires pain and sweat followed by calculations that may make take weeks using hundreds of billions of photons, as was done for the terrestrial radiation calculations for the horizontally heterogeneous cloud field discussed in Section 6.4.4.

6.3.6 Irradiance, Flux Divergence, Radiance, and Path Lengths

Previous subsections have dealt mostly with how to trace the life histories of photons imagined to be injected into a medium, then scattered or absorbed according to probabilistic equations. These histories then lead to the measurable physical quantities to which we now turn.

Irradiance

For problems in which a scattering and absorbing medium is illuminated by a source of radiation external to it, the general method for estimating irradiances is as follows. The medium of interest could lie within a domain one bounding surface of which is illuminated by irradiance F_i within some spectral interval. Illumination of more than one surface poses no special difficulties, just more bookkeeping. For example, for solar radiation in the atmosphere, F_i could be the solar irradiance in a spectral interval times the cosine of the solar zenith angle, the illuminated surface a horizontal plane at an altitude taken to be the top of the atmosphere. A finite cloud would in general be illuminated on more than one surface. The total spectral power incident on an illuminated boundary with area A_i is $F_\mathrm{i}A_\mathrm{i}$. Although the incident illumination often is taken to be uniform across A_i, this restriction could be removed by dividing A_i into smaller areas over each of which the illumination is uniform. For example, the bounding surface of a spherical cloud (why not?) could be divided into small areas over each of which the irradiance is different but approximately uniform. If N_b photons are considered to be launched at random across A_i, the incident power per photon is

$$P_\mathrm{b} = \frac{F_\mathrm{i}A_\mathrm{i}}{N_\mathrm{b}}. \tag{6.90}$$

This is not the power *of* a photon, a meaningless concept. Although we say that we inject photons into a medium, an intuitively helpful way of speaking, in a strict sense they are bundles of energy or power, and so in what follows we sometimes use the term bundle when we want to make the distinction. Each time a bundle crosses a specified area A within the domain, P_b is added to the bank account for that area. We keep track of the sense in which bundles cross A because in general the irradiance there has two senses defined by two hemispheres of directions. If at the end of a calculation N_A bundles crossed A in a given sense, the total irradiance there is

$$F_\mathrm{A} = \frac{N_\mathrm{A}P_\mathrm{b}}{A} = \frac{N_\mathrm{A}F_\mathrm{i}A_\mathrm{i}}{N_\mathrm{b}A}. \tag{6.91}$$

If more than one bounding surface of the domain is illuminated, $F_\mathrm{i}A_\mathrm{i}$ becomes a sum over each surface. Moreover, one could keep track of the separate contributions of bundles that cross each bounding surface to the physical quantity of interest. If the incident radiation is monodirectional, a single bounding surface is sufficient, and is mathematically equivalent to many surfaces, provided the surface is sufficiently large that the bundles that cross it are equally likely to enter the medium anywhere.

Flux Divergence

Because the rate at which radiant energy is absorbed per unit volume is the negative divergence of the vector irradiance [Eq. (6.18)], we can calculate this quantity directly with the Monte Carlo method. If N_V power bundles out of a total of N_b are absorbed within a volume V

$$-(\nabla \cdot F_\mathrm{V})_\mathrm{V} = \frac{N_\mathrm{V}P_\mathrm{b}}{V} = \frac{N_\mathrm{V}F_\mathrm{i}A_\mathrm{i}}{N_\mathrm{b}V}. \tag{6.92}$$

Again, if illumination is over more than one bounding surface, $F_\mathrm{i}A_\mathrm{i}$ becomes a sum. Equations (6.91) and (6.92) are similar in form. The quantity $F_\mathrm{i}A_\mathrm{i}$ is a boundary condition, A and V are geometrical quantities specified to taste, and hence the only quantity to be calculated is a ratio of numbers, $N_\mathrm{A}/N_\mathrm{b}$ or $N_\mathrm{V}/N_\mathrm{b}$.

Radiance

Radiances and path lengths are more difficult to calculate by Monte Carlo methods than are irradiances and flux divergences. If we were to naively attempt to estimate the radiance in a particular direction at a point by counting the bundles that cross a small area around that point in a small set of directions around that direction, the computations would take a very long time to yield statistically meaningful results. This is because only a small fraction of bundles, in general, would lie within this set of directions, and so a great number of incident bundles would be needed to reduce the statistical spread (variance). To avoid this problem we use a variance reduction technique: a method for extracting more information from each bundle than by simply tracing each bundle through the domain, thereby reducing noise in the results.

The easiest way to explain the essence of this technique is to consider a simple problem: estimating the vertical radiance distribution at the top of a rectangular, negligibly absorbing cloud illuminated at normal incidence. Power bundles are incident at random points on the top surface A_i of this cloud. An incident bundle travels a certain distance specified by choosing a random number, then scatters in a direction determined by choosing other random numbers. Denote by $\vartheta_{\mathrm{s}1}$ the first scattering angle and by $\varphi_{\mathrm{s}1}$ the first azimuthal angle. We also can determine a scattering angle ϑ_1 and azimuthal angle φ_1 such that the bundle would be scattered vertically upward. The power scattered per unit solid angle in this hypothetical scattering event and transmitted to the top surface is

$$P_\mathrm{b}\, p(\vartheta_1, \varphi_1) \exp(-\tau_1), \tag{6.93}$$

where τ_1 is the optical thickness of the path between the point of scattering and the top surface. The bundle trajectory intersects this surface at a point, and we record its coordinates and the associated power per unit solid angle [Eq. (6.93)], which is proportional to its contribution to the vertical radiance. Now return to the point of first scattering, pick random numbers to determine the distance to the next scattering event and the next scattering direction, and again determine the amount of radiation per unit solid angle scattered vertically and transmitted to the surface. Continue in this vein until the bundle exits the medium. If many bundles are incident randomly across the top surface, the mathematical result is a surface non-uniformly peppered with points (Fig. 6.7). Any planar area A_k on this surface encloses a subset of these points. To obtain an estimate of the average vertical radiance over this area, divide the sum of all terms of the form Eq. (6.93) by A_k:

$$L_\mathrm{k} = \frac{P_\mathrm{b}}{A_\mathrm{k}} \sum_{j=1}^{N_\mathrm{k}} p(\vartheta_j, \varphi_j) \exp(-\tau_j) = \frac{F_\mathrm{i}A_\mathrm{i}}{A_\mathrm{k}N_\mathrm{b}} \sum_{j=1}^{N_\mathrm{k}} p(\vartheta_j, \varphi_j) \exp(-\tau_j), \tag{6.94}$$

where the sum is over all N_k points lying within A_k. This sum embodies all the different ways bundles can contribute to the vertical radiance within A_k.

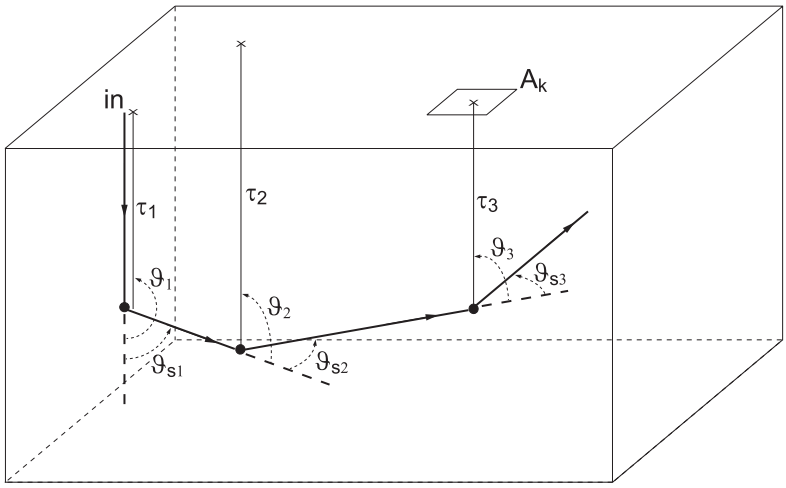

Figure 6.7: Incident power bundles are scattered at various points and in various directions ϑ_{sj} determined by choosing random numbers. At each of these points we can determine the contribution to the radiance at the top surface, an optical distance τ_j, if a bundle had been scattered in the direction ϑ_j such that it is perpendicular to this surface. Many incident bundles result in a surface peppered with points, only three of which are shown. The number of points enclosed within any area A_k is proportional to the average radiance (here vertical) over this area.

To make this clearer, we reconsider the first scattering event. Although the scattering angle was ϑ_{s1}, it *could* have been ϑ_1, because both angles are chosen in the same way, with a random number. Similarly, we could have chosen a random number that gave at least a value τ_1, an optical thickness such that a vertical bundle would be transmitted to the surface. The same arguments hold at the point of the second scattering event, the third, and so on. Thus the sum in Eq. (6.94) is taken over many physically possible ways in which a bundle could emerge vertically from the top surface. Choose enough random numbers specifying directions and distances and most of these would be realized.

For N_b sufficiently large, N_k is approximately proportional to N_b, and to A_k if it is sufficiently large. We must choose the ratio A_k/A_i to be sufficiently large so that we obtain a good estimate of the radiance, but not so large that this is not a local radiance. For example, if $A_k/A_i = 1$, Eq. (6.94) would yield an average vertical radiance over the entire top surface. The downward radiance below cloud is calculated in the same way. For oblique incidence and radiances other than in the vertical, the procedure is the same, the bookkeeping more cumbersome. Choose a desired direction for the radiance at the upper or lower surface, determine the intersection points of bundles in that direction with these surfaces, calculate quantities of the form Eq. (6.93), and sum over all of them associated with points lying within some area. To obtain the radiance divide this sum by this area projected onto the radiance direction. More complicated geometries can be treated at the expense of more complicated bookkeeping. Clouds of strange and wondrous shapes could be treated by imagining them to be enclosed in rectangular boxes illuminated by a specified radiation field. Calculate the

radiance distribution over the box and use the radiance invariance principle to extrapolate to points on the cloud surface.

Photon Path Length Distributions

Many photon path length distributions are possible depending on whatever conditions we impose. The simplest example is a plane-parallel medium illuminated at an arbitrary angle. With the Monte Carlo method we can keep track of the total path lengths, from entry point to exit point, of bundles that emerge from the medium at its upper or lower boundaries. Each bundle yields a different path length. We pay no heed to the directions at which the bundles emerge. We keep track of these path lengths and assign them to bins of specified width. Divide the number of times a path length falls within a particular bin by the bin width to obtain an estimate of the continuous probability distribution for photon paths. All these path lengths are equally weighted.

But suppose we wanted to restrict ourselves to path lengths of only those bundles that emerge in a particular direction, the vertical, say, for a given illumination. We could proceed as we did in the previous subsection about radiances. At each scattering point, we know the total path length up to that point and the vertical path length to the surface. Weight the sum of the total path length to the scattering point and the vertical path length by the associated radiance. Do this for an incident bundle until it emerges from the medium. Repeat again and again, and then divide the set of path lengths by the sum of all radiances. This gives a radiance-weighted set of path lengths for those bundles that contribute to the vertical radiance at the top (or bottom) surface. Bin all these path lengths and divide the number in each bin by the bin width to obtain the probability distribution.

We could be even more specific and determine the path length distribution corresponding to all bundles that enter a medium, which need not be plane-parallel, only within a specified area, and emerge in a particular direction through yet another specified area. Thus there is no such thing as *the* photon path length distribution but rather many such distributions, one for each set of constraints imposed on incident and exiting photons. All these distributions may bear a family resemblance for a given medium but they will not be identical.

6.4 Atmospheric Applications of the Monte Carlo Method

The Monte Carlo method can be applied to many problems of radiative transfer in planetary atmospheres. In the following sections we give a sample of such applications. We begin with irradiances in plane-parallel media, which are amenable to treatment by other methods, then show photon path length distributions, reflection and transmission by finite clouds, and finally irradiance, flux divergence, and heating rate profiles in a clear and in a horizontally heterogeneous cloudy atmosphere. For all these Monte Carlo calculations, the Henyey–Greenstein phase function (Sec. 6.3.2) was used.

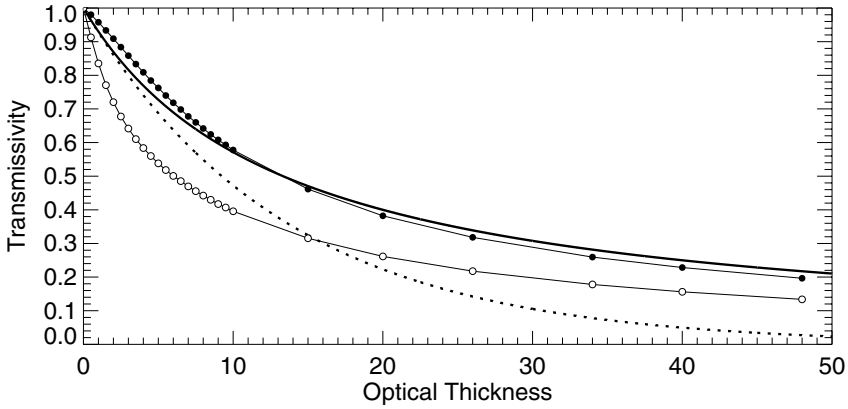

Figure 6.8: Transmissivity of a plane-parallel medium above a nonreflecting surface. The dotted curve is exponential attenuation, the thick solid curve with no circles is from the two-stream theory, and the solid circles are Monte Carlo calculations, all for an overhead sun. Open circles are Monte Carlo calculations for a 60° solar zenith angle. The asymmetry parameter is 0.85.

6.4.1 Irradiances in Plane-Parallel Media

Perhaps the simplest Monte Carlo calculations are of irradiances reflected by , transmitted by, and within a plane-parallel medium. An incident photon that emerges at any direction from the illuminated (top) boundary of such a medium is counted as contributing to the reflectivity, and we are spared the bother of keeping track of this direction. And similarly for photons emerging from the bottom boundary.

Figure 6.8 shows the transmissivity of a negligibly absorbing medium with properties similar to those of clouds at visible wavelengths calculated by the Monte Carlo method and compared with that calculated by the two-stream theory of Section 5.2. The two methods yield almost identical results, which gives us some confidence in the simple two-stream theory. Of course, this theory is limited to normal incidence, whereas the Monte Carlo method is indifferent to the direction of the incident photons. Figure 6.8 also shows transmissivity for a 60° solar zenith angle, which is never greater than that for overhead illumination. Can you give a simple physical explanation for this?

Monte Carlo calculations of the diffuse irradiance transmitted by a cloud are no more difficult than calculations of the total transmitted irradiance: incident photons that make a direct transit through the cloud are not counted as contributing to the diffuse irradiance. Figure 6.9 shows the diffuse downward irradiance below a plane-parallel medium (cloud) calculated by the Monte Carlo method and compared with that calculated by the two-stream theory. The agreement is quite good. Again, the two-stream theory is limited to normal incidence whereas the Monte Carlo method is not. This figure also shows the diffuse downward irradiance for a 60° solar zenith angle, which is greater than that for 0° illumination except at the smallest optical thicknesses.

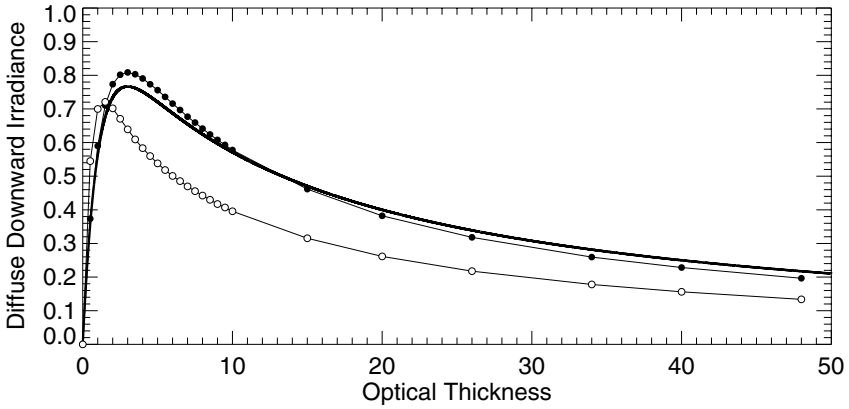

Figure 6.9: Diffuse downward irradiance normalized by the incident irradiance from the two-stream theory (thick solid line with no circles) and Monte Carlo calculations (solid circles) for an overhead sun. Open circles are Monte Carlo calculations for a 60° solar zenith angle. The asymmetry parameter is 0.85 and the medium is above a non-reflecting surface.

Figure 6.8 shows total transmissivity and Fig. 6.9 diffuse transmissivity. For small optical thickness ($\approx$0) the two are quite different: $\approx$1 for the former, $\approx$0 for the latter. With increasing optical thickness the two approach each other, as expected. For sufficiently large optical thickness essentially all the transmitted radiation is diffuse because of exponential attenuation of the direct radiation.

According to the two-stream theory, both upward and downward irradiances within a negligibly absorbing medium decrease linearly with increasing optical depth. The Monte Carlo calculations in Fig. 6.10, however, show that both irradiance profiles display some curvature, especially near the upper boundary. Moreover, for an optically thick medium, the curvature can be so extreme that the downward irradiance within the cloud can exceed the incident irradiance. This does not violate conservation of energy, which requires only that the difference between the two irradiances be constant with optical depth and the downward irradiance never be less than the upward, conditions the irradiances in Fig. 6.10 do indeed satisfy. But as Fig. 6.11 shows, this increase of the downward irradiance above the incident irradiance near the upper boundary occurs only for illumination near normal incidence.

Real clouds – horizontally and vertically inhomogeneous and without sharp boundaries – are vastly more complicated than mathematical clouds, and calculating irradiances within and outside such clouds is much easier than measuring these quantities for real clouds. How well do calculated irradiances compare with measured irradiances? Figure 6.12 shows irradiances in the middle of the visible spectrum for a stratocumulus cloud about 700 m thick and with an estimated optical thickness of 10–20. Unlike the mathematical clouds for which previous calculations were done, this real cloud is not vertically homogeneous. Nevertheless, the upward and downward measured irradiances are not jarringly different from the calculated ones. Both upward and downward irradiances decrease approximately linearly with increasing op-

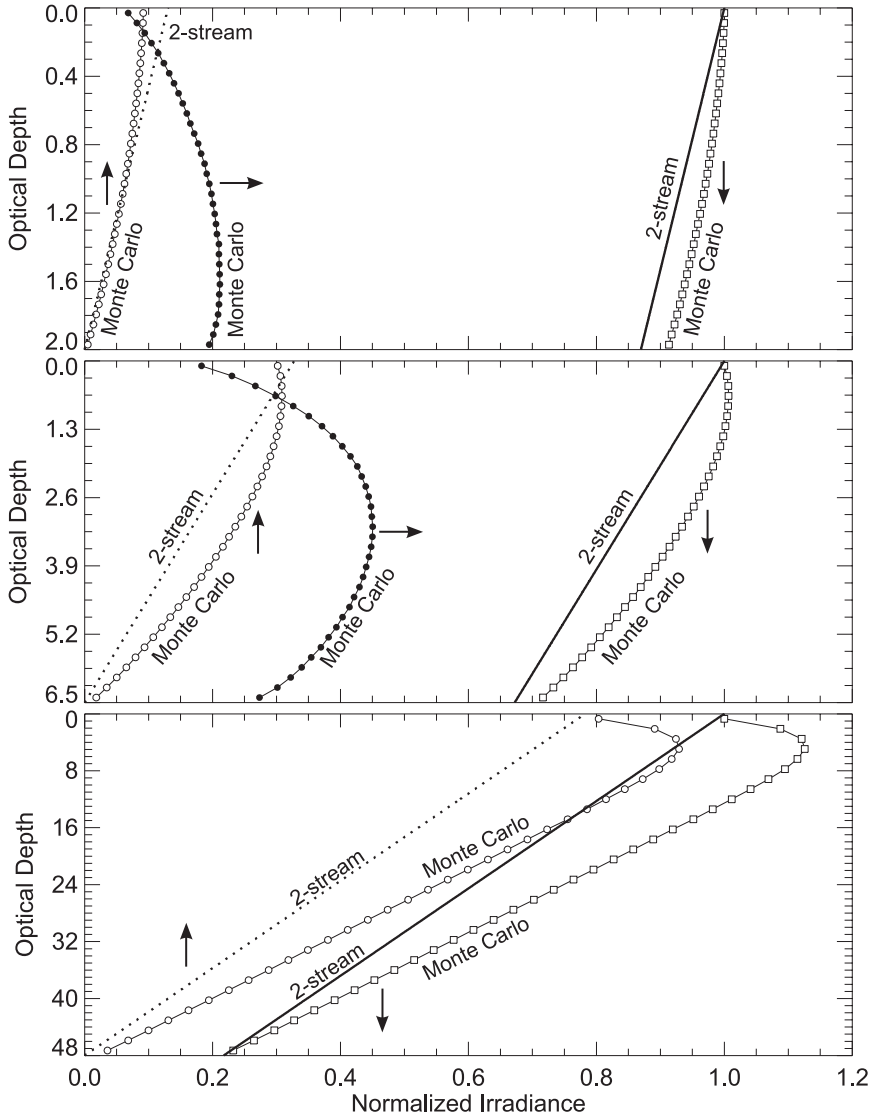

Figure 6.10: Downward (↓) and upward (↑) normalized irradiances within negligibly absorbing clouds of optical thickness 2 (top), 6.5 (center), and 48 (bottom) from two-stream theory and the Monte Carlo method. The asymmetry parameter is 0.85, the sun is overhead, and the surface below the clouds is nonreflecting. Horizontal irradiances are denoted by →.

tical depth, the downward irradiance is greater than the upward, and the difference between them is approximately constant. And the relative difference between them is in rough accord with what we would expect from Fig. 6.10, which shows a steadily decreasing relative differ-

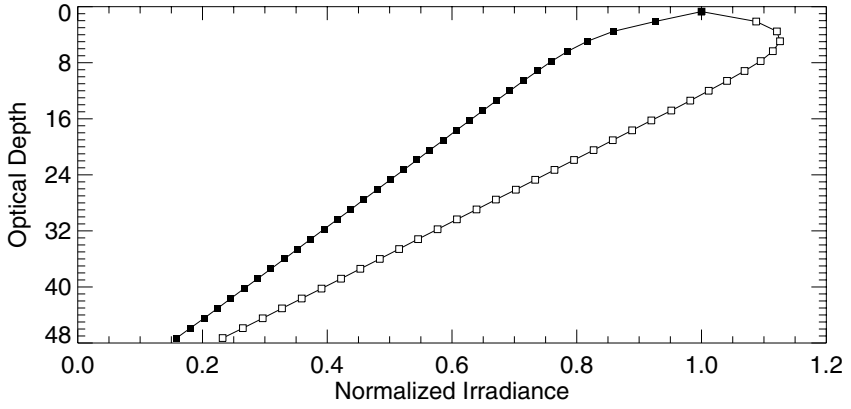

Figure 6.11: Downward normalized irradiance within a negligibly absorbing cloud with total optical thickness 48 and asymmetry parameter 0.85 calculated by the Monte Carlo method. Open squares are for the sun overhead, solid squares for 60° solar zenith angle. The surface below cloud is nonreflecting.

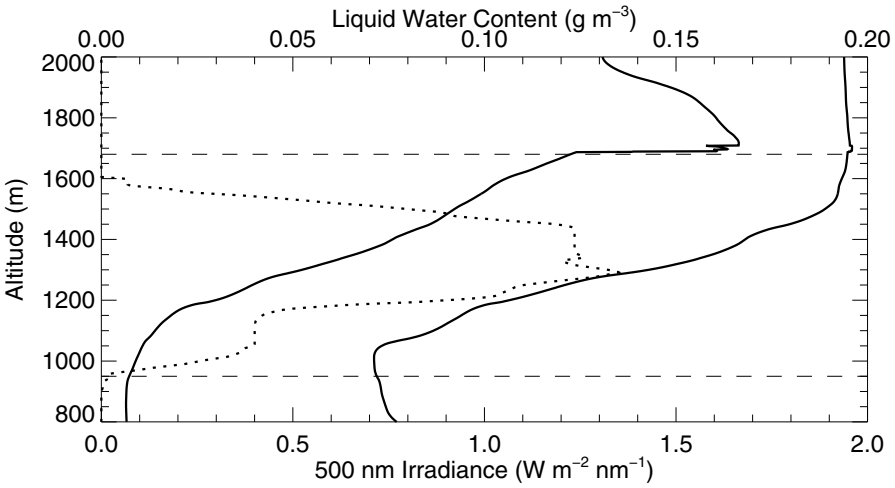

Figure 6.12: Measured downward (right solid curve) and upward (left solid curve) irradiances at 500 nm within a stratocumulus cloud between about 950 m and 1700 m (dashed lines). The solar zenith angle was approximately 10°. The dotted curve is liquid water content. These curves were obtained from as-yet unpublished measurements provided by Peter Pilewskie.

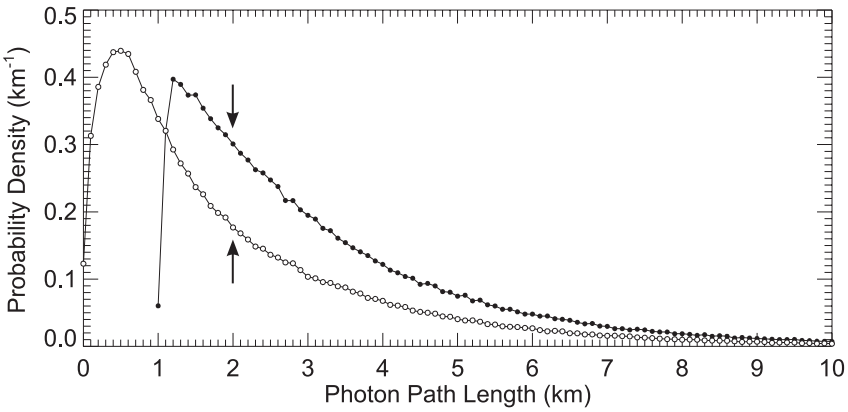

Figure 6.13: Probability density for path lengths of photons that contribute to the downward radiance below cloud (↓) and to the upward radiance above cloud (↑). The incident radiation is normal to a plane-parallel cloud of physical thickness 1 km, scattering mean free path 1/16 km, and asymmetry parameter 0.75. The cloud overlies nonreflecting ground.

ence with increasing optical thickness, about 80% for an optical thickness of 2, about 60% for an optical thickness 6.5, and about 20% for an optical thickness of 48, whereas the relative difference is about 40% for the real cloud with an estimated optical thickness of 10–20.

6.4.2 Photon Path Lengths

Everything takes time. Nothing occurs in an instant. And yet up to this point time has been absent from our analyses. We have implicitly assumed, for example, that reflected photons appear instantaneously at a detector when a cloud is illuminated. This is usually an acceptable fiction because relevant distances, say of order kilometers, divided by the speed of light correspond to times of order millionths of a second. But suppose that a cloud is illuminated by a short duration pulse, as from a laser beam. A pulse width in length units may be of order 100 m, which corresponds to a pulse width in time units of order 0.1 μs. We may think of an idealized pulse as having a square shape: the beam is turned on instantaneously, is constant for a fixed time (pulse width), then is turned off instantaneously. Suppose that such a pulse illuminates a cloud illuminated at normal incidence. What is the shape of the reflected pulse in the backward direction and the transmitted pulse in the forward direction? All photons that contribute to the reflected and transmitted radiances are born equal but do not suffer the same fates in the cloud. Because "time and chance happeneth to them all" pulses are broadened or stretched by an amount depending on the scattering properties of the cloud. Calculating this pulse broadening is a task to which the Monte Carlo method is well suited.

Figure 6.13 shows calculated probability distributions of path lengths for those normally incident photons that contribute to the upward radiance above a plane-parallel cloud and to the downward radiance below the cloud; the negligibly absorbing cloud is 1 km thick with a scattering mean free path 1/16 km and asymmetry parameter 0.75. The most probable path length of photons contributing to the downward radiance is close to 1 km. Most of this ra-

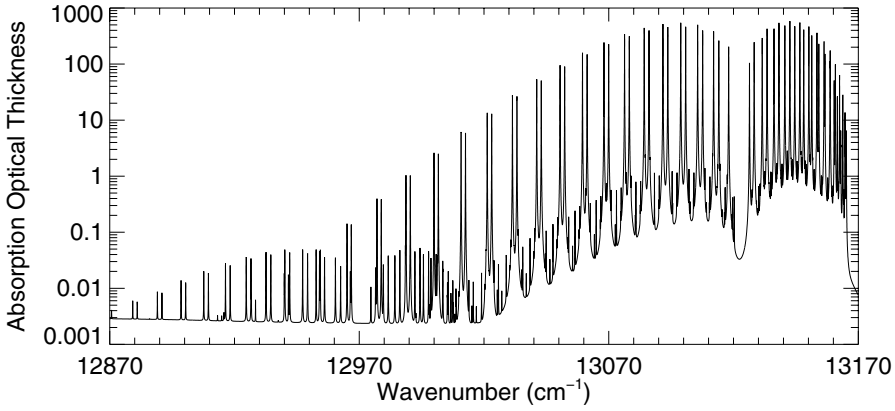

Figure 6.14: Absorption optical thickness of oxygen for 100 km of Earth's atmosphere. From Qilong Min.

diance comes from photons that make a direct path through the cloud. The most probable path length of photons contributing to the upward radiance is about half the thickness of the cloud. For both radiances the pulse is stretched considerably, about a factor of 20 or so for a pulse width of 100 m. Pulse broadening sets an upper limit on the pulse repetition rate (time between pulses) but also contains information about the cloud.

Photon path length distributions also can help us understand atmospheric radiative transfer. As an example, we consider upward and downward radiances at two adjacent wavenumbers in the near-infrared (wavelengths near 770 nm) where absorption in Earth's clear atmosphere is mostly by molecular oxygen. The absorption optical thickness of oxygen up to an altitude of 100 km is shown in Fig. 6.14. At wavenumber 12970 cm^{-1} the absorption optical thickness is negligible whereas at the nearby wavenumber 12965 cm^{-1} the absorption optical thickness is about 0.11. Monte Carlo calculations of the relative radiance difference $(L_\mathrm{a} - L_\mathrm{n})/L_\mathrm{n}$, where L_a is the radiance at the absorbing wavenumber and L_n is the radiance at the negligibly absorbing wavenumber, for the upward radiance at 100 km and the downward radiance at 0 km are shown in Fig. 6.15 for clear sky, a cloudy sky with a single cloud of scattering optical thickness 16 between 1.0 km and 1.6 km, and a cloudy sky with same total optical thickness but distributed differently: a low cloud of scattering optical thickness 8 between 1.0 km and 1.6 km and a high cloud of optical thickness 8 between 8.6 km and 10 km. The cloud is negligibly absorbing and has an asymmetry parameter 0.75.

For the clear sky the relative radiance difference at the two adjacent wavenumbers is almost the same, about 10%, for the upward (100 km) and downward (0 km) radiances and is negative because radiances are less at the absorbing wavenumber. A single low cloud changes these results: both relative radiance differences increase in magnitude and by approximately the same amount. But the same total cloud, when distributed equally between high and low altitudes, decreases the magnitude of the relative upward radiance difference and markedly increases the magnitude of the relative downward radiance difference. Why?

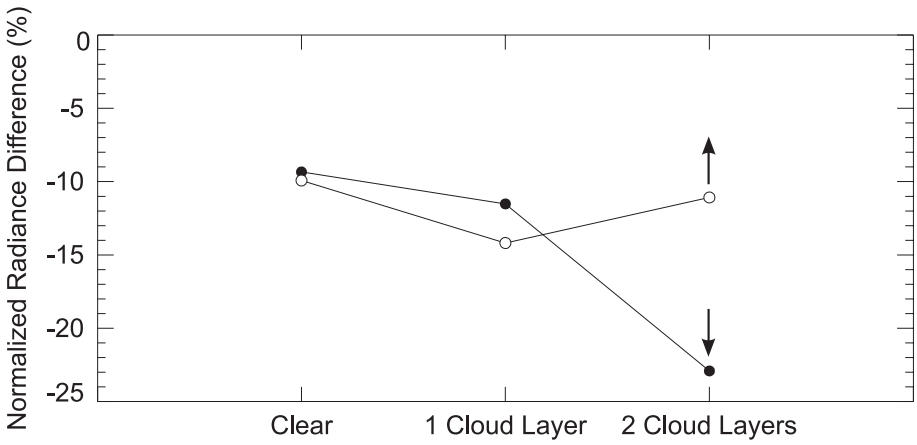

Figure 6.15: Relative difference of radiances at two adjacent wavenumbers in the near-infrared, one for which absorption is negligible and one for which the absorption optical thickness, a consequence of absorption by molecular oxygen, is 0.11. This difference for the upward radiance at 100 km is denoted by $\uparrow$, that for the downward radiance at 0 km is denoted by $\downarrow$. The cloud layers are negligibly absorbing and have the same total optical thickness (16) but are distributed differently: a single layer between 1.0 km and 1.6 km and two layers of equal optical thickness, one between 1.0 km and 1.6 km, one between 8.6 km and 10 km.

To answer this we appeal to photon path length distributions. Figure 6.16 shows distributions for photons that contribute to the downward radiance at the negligibly absorbing wavenumber for the clear and two cloudy skies and at the absorbing waveneumber for the cloudy sky with equal optical thickness low and high clouds. The source of illumination is at 100 km and is normal to the plane-parallel atmosphere.

For the clear sky almost all path lengths of photons that contribute to the downward radiance are 100 km and hence so is the average path length. A single cloud layer changes the distribution but not by much. Two widely separated cloud layers, however, markedly change the photon path length distribution because of multiple scattering within each cloud and, more important, multiple scattering between clouds. This is why the downward radiance at the absorbing wavelength decreases. Longer path lengths expose photons to more chances of being absorbed by molecular oxygen.

The magnitude of the upward relative radiance difference with two cloud layers is less than that with one cloud because scattering by the high altitude cloud shields some incident photons from the most absorbing part of the atmosphere. Also shown in Fig. 6.16 is the photon path length distribution for the downward radiance at the absorbing wavenumber, which is not appreciably different from that at the negligibly absorbing wavenumber. Thus although we show mostly photon path length distributions at the negligibly absorbing wavenumber, our conclusions are valid for both wavenumbers.

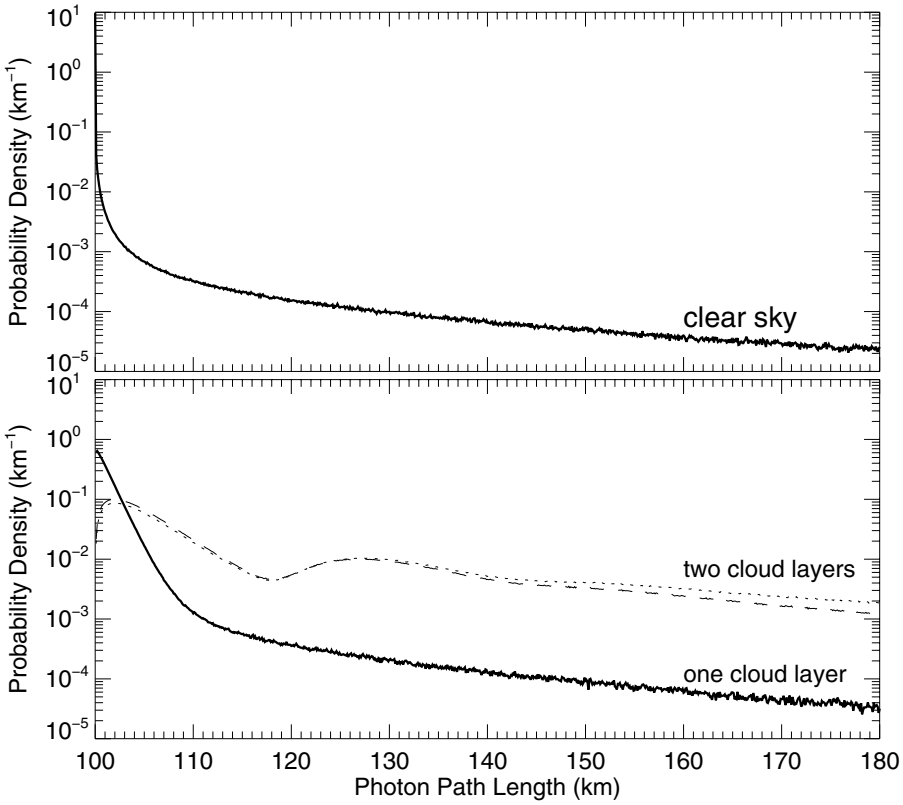

Figure 6.16: Path length distributions for photons contributing to the downward radiance at the ground for clear sky and two cloudy skies, one with a negligibly absorbing cloud between 1.0 km and 1.6 km, and one with two clouds of the same total optical thickness (16) equally shared by a low cloud (1.0–1.6 km) and a high cloud (8.6–10 km). Radiation is normally incident on a plane-parallel atmosphere at 100 km. Except for the dashed curve in the bottom panel, the wavenumber is that for which absorption is negligible. For the dashed curve, the molecular oxygen optical thickness is 0.11.

6.4.3 Three-dimensional Clouds

The qualifier "three-dimensional" is in a sense redundant give that *all* clouds are three-dimensional. Their properties vary in all three spatial directions. A cloud with properties varying in only one direction is a figment of the imagination of modelers. A one-dimensional cloud is an idealization never realized in nature. This should always be kept in mind when assessing the pronouncements of modelers, who sometimes confuse model clouds with real ones. Plane-parallel homogeneous clouds are so much easier to deal with. Even though they don't exist, they ought to. Nor do rectangular clouds exist, but they are a closer match to those that do.

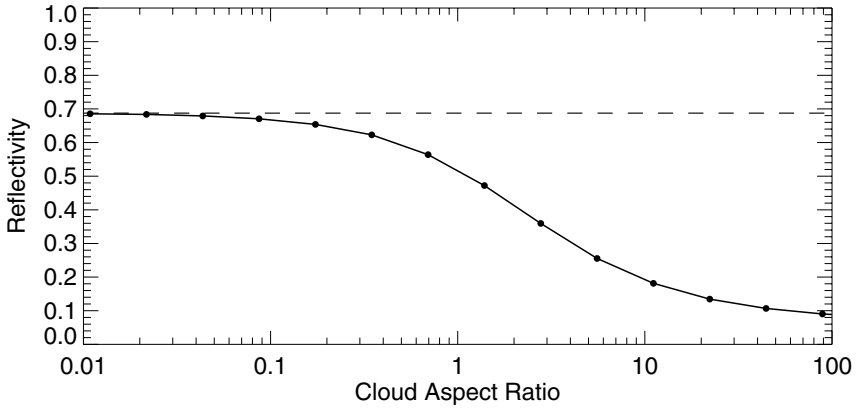

Figure 6.17: Reflectivity (solid curve) for normal incidence of a negligibly absorbing columnar cloud with square cross section, vertical optical thickness 16, overlying a nonreflecting surface. The aspect ratio is the vertical geometrical thickness of the cloud relative to the length of its side. Reflectivity (dashed curve) of a cloud with the same vertical optical thickness but infinite in lateral extent. The asymmetry parameter is 0.75.

Figure 6.17 shows the reflectivity of a square columnar cloud of fixed vertical optical thickness but varying aspect ratio, the ratio of its geometrical thickness to the length of one of its sides. Absorption is negligible, the ground below cloud is non-reflecting, and incident radiation is vertically downward. For a sufficiently small aspect ratio, the reflectivity is close to that for a cloud infinite in lateral extent. For aspect ratios greater than about 1, the difference between a finite and an infinite cloud, otherwise identical, becomes appreciable. For large aspect ratios the reflectivity plunges because of leakage of photons out the sides of the cloud. You can observe the consequences of this while flying over a field of broken clouds, all with about the same vertical thickness but different lateral dimensions. The larger clouds are brighter than the smaller clouds, not because they mysteriously have become corrupted by some highly absorbing pollutant (an explanation we have encountered) but because leakage out the sides of a cloud is equivalent to absorption within it.

Figure 6.18 shows how leaked photons contribute to the irradiance distribution below cloud. For the highest aspect ratio (11), little radiation is transmitted into the geometrical shadow of the cloud, most incident radiation either reflected or transmitted through the sides. For the smallest aspect ratio (0.09), the irradiance in the shadow of the cloud is almost what would be transmitted if the cloud were infinite in lateral extent. For an appreciable distance beyond the geometrical shadow of this cloud the downward irradiance is 5–10% greater than the clear sky value. See Problem 4.15 for more about irradiances greater than clear sky values on days with broken clouds.

Now we turn to vertical radiances above and below cloud. Again, the physical thickness is 1 km, the optical thickness 16. Figure 6.19 shows radiances for clouds with four aspect ratios. For small aspect ratios ($\ll 1$), the radiance hardly varies from cloud center to edge. And this is also true for large aspect ratios (> 1), although the magnitude of the radiance is

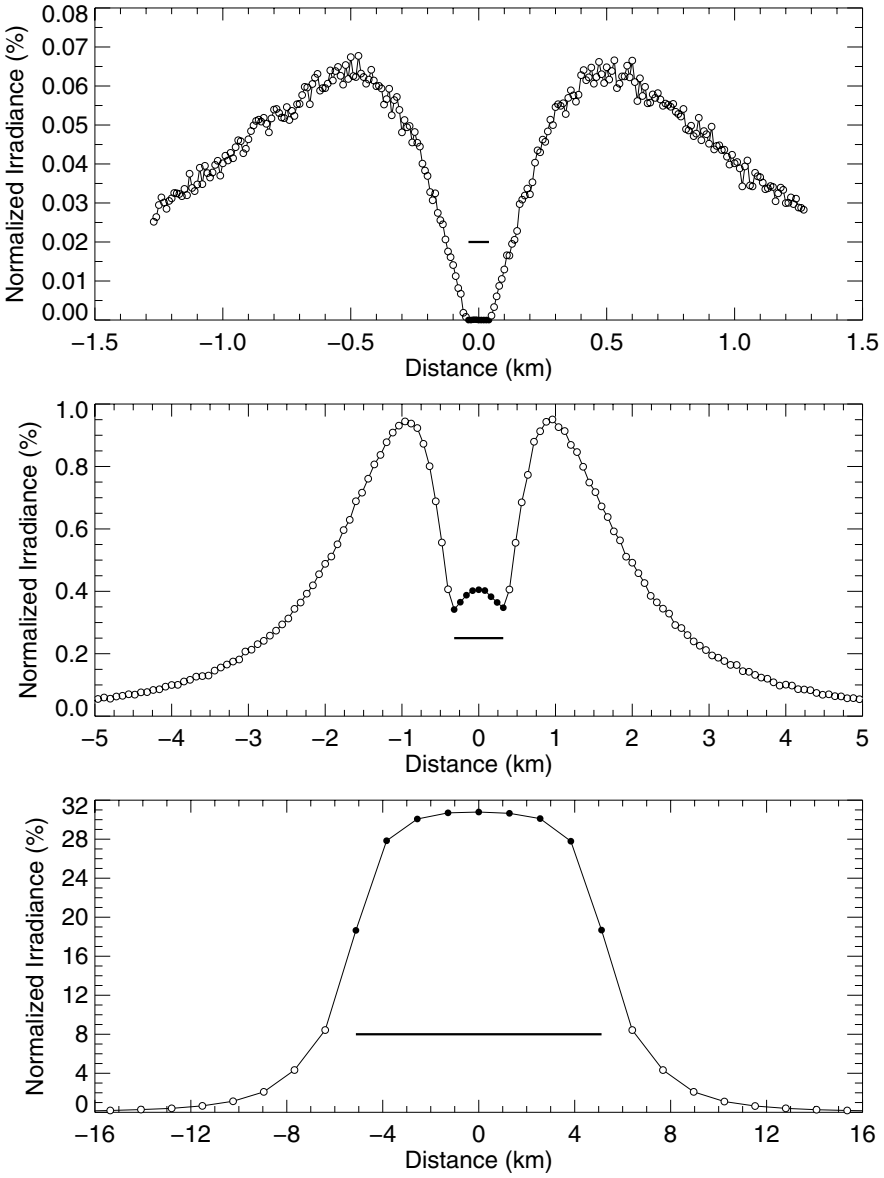

Figure 6.18: Downward irradiance distribution along a line formed by the intersection with the ground of a vertical plane through the center of columnar clouds 1 km thick with vertical optical thickness 16 and asymmetry parameter 0.75 but different aspect ratios: 11 (top), 1.4 (middle), 0.09 (bottom). The incident radiation is directly overhead and the irradiances are normalized by the incident irradiance. Outside the geometrical shadow region, shown by horizontal lines, the incident irradiance is subtracted from the total (open circles).

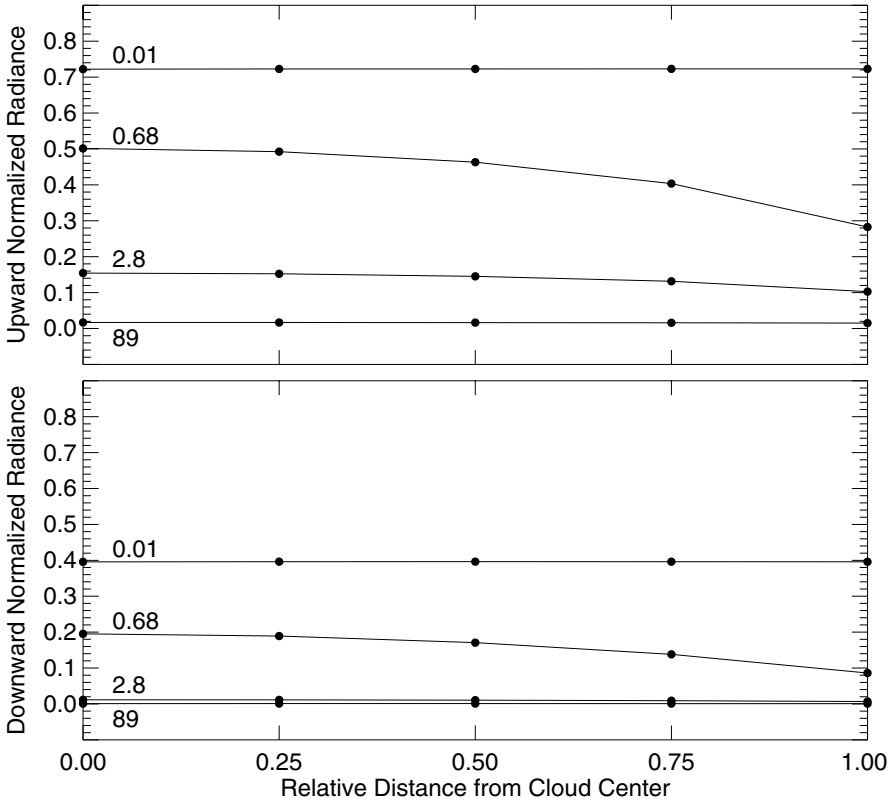

Figure 6.19: Upward radiance above and downward radiance below square clouds 1 km thick with vertical optical thickness 16 and asymmetry parameter 0.75 and with the aspect ratios indicated. The horizontal axis is the position along a line formed by the intersection of a vertical plane through cloud center with the top and bottom boundaries. Cloud center is indicated by 0, cloud edge by 1. The downward radiances for the two largest aspect ratios are nearly identical. The normalization factor is the radiance of a diffuse reflector with reflectivity 1. Radiances calculated by Jonathan Petters for a plane-parallel cloud and a one-dimensional solution to the radiative transfer equation agree to at least three digits with Monte Carlo calculations for the 0.01 aspect ratio cloud.

much smaller. For an aspect ratio near 1, however, the gradient of radiance is appreciable, with higher radiances near the center than near the edge. This can be observed flying over broken clouds with comparable vertical and horizontal dimensions, and has nothing fundamental to do with a possibly different drop size distribution and liquid water content near cloud edge. For the almost plane-parallel cloud (smallest aspect ratio), we can estimate the vertical radiance by other than the Monte Carlo method. Radiances obtained both ways are in agreement, which gives us confidence that the scheme outlined in Section 6.3.6 for estimating radiances is sound.

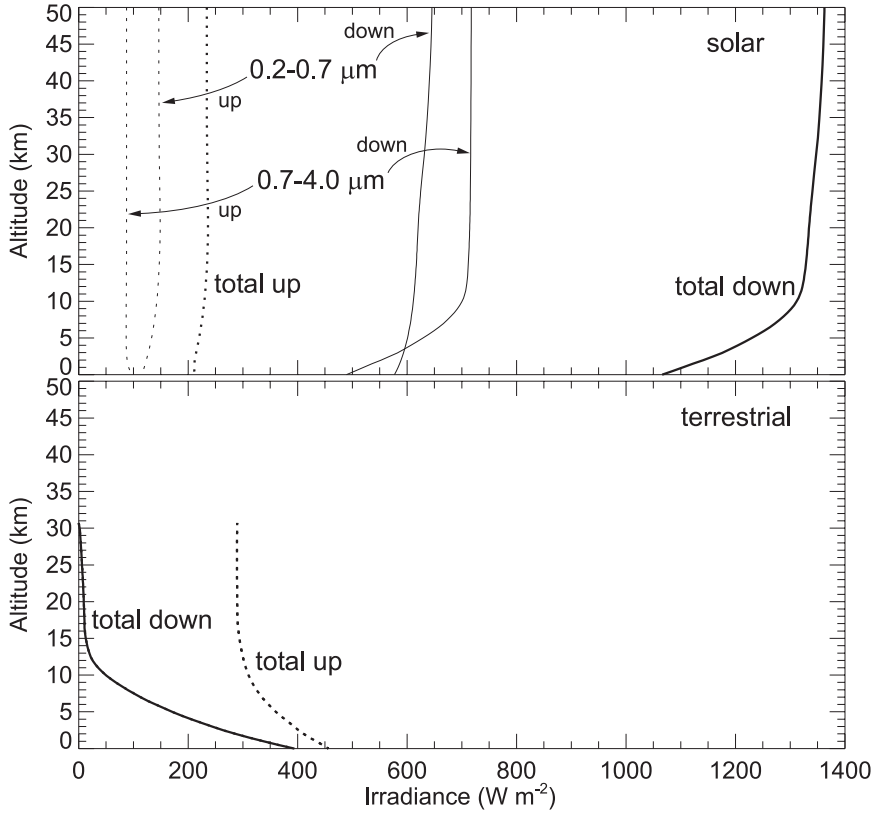

Figure 6.20: Monte Carlo calculations of downward and upward solar (top) and terrestrial (bottom) irradiance profiles for a typical tropical clear-sky atmosphere. Temperature and moisture profiles from Barker *et al.* (2003). The sun is overhead and the reflectivity of the diffusely reflecting ground is 0.2 over the solar spectrum. Terrestrial irradiances calculated using a standard method for plane-parallel media are indistinguishable from these Monte Carlo calculations. Terrestrial radiation results from Cole (2005).

6.4.4 Solar and Terrestrial Irradiances, Flux Divergences, and Heating Rate Profiles

For Earth's thermodynamic internal energy to be constant over a sufficiently long time (e.g., a year) solar radiation absorbed by Earth must be equal to terrestrial radiation emitted by it. This was expressed by the radiative equilibrium equations in Section 1.6. These are what might be called zero-dimensional or global equations, specifying how *much* is absorbed and emitted but not *where*. Now we turn to "where" in the atmosphere but only in one dimension, the vertical.

Figure 6.20 shows Monte Carlo calculations of downward and upward solar and terrestrial irradiance profiles in a clear sky for a temperature and moisture profile typical of the tropics.

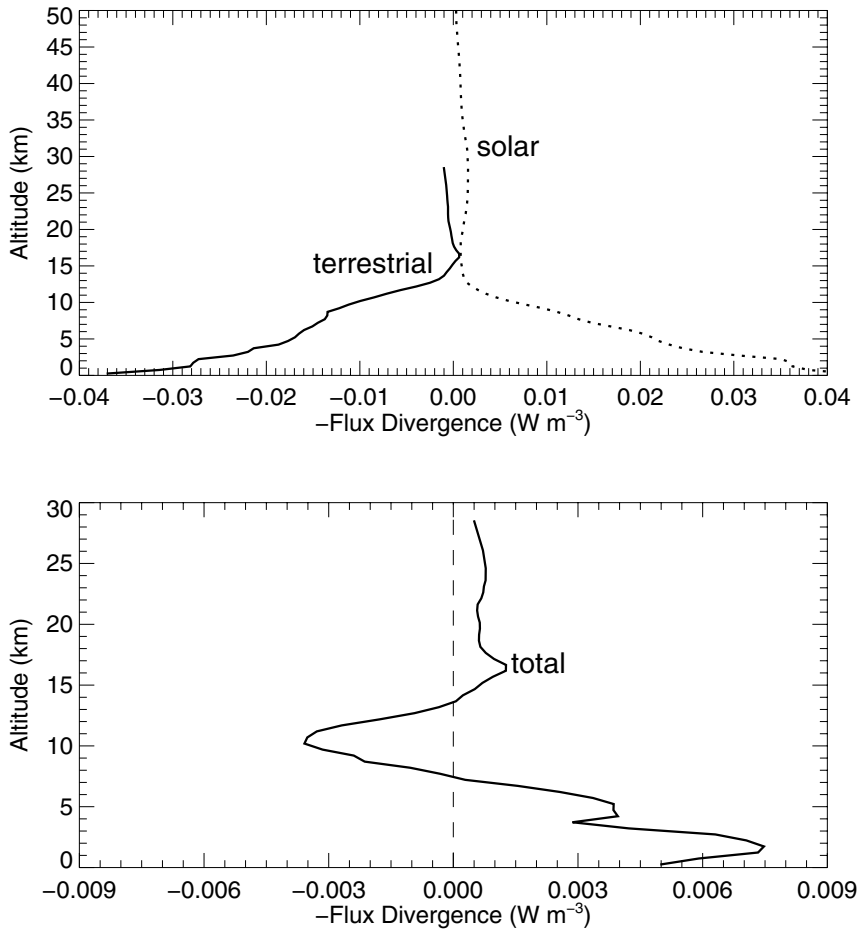

Figure 6.21: Solar, terrestrial, and total *negative* flux divergences corresponding to the irradiances in Fig. 6.20. Positive values correspond to net heating, negative to net cooling. Note the change in both horizontal and vertical scales between the two panels. Terrestrial radiation results provided by Jason Cole.

Separate profiles are shown for the solar irradiance between 0.2 μm and 0.7 μm, denoted for brevity as visible, and between 0.7 μm and 4.0 μm, denoted as infrared. The sharp decrease in the downward solar infrared irradiance below 10 km must be a consequence of absorption by something because the scattering optical thickness of the atmosphere is so small at these wavelengths. Figure 2.12 indicates that the likely culprit is water vapor. Between about 50 km and 15 km the visible downward irradiance decreases faster than the infrared irradiance because of absorption of ultraviolet (0.2–0.3 μm) radiation by ozone. The visible upward irradiance

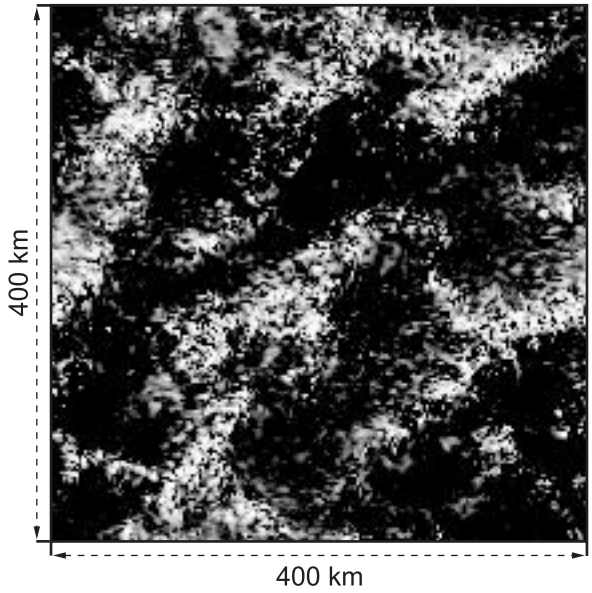

Figure 6.22: Depiction by shading of spatially varying integrated cloud liquid water content, from the surface to about 100 km, obtained from model calculations by Grabowski et al. (1998). The higher the brightness, the higher the liquid water content. The horizontal resolution is 2 km.

from 15 km to 50 km does not decrease with increasing altitude because most of the photons that ozone could absorb are removed on their downward trip through the atmosphere.

The irradiances in Fig. 6.20 as well as the flux divergences and heating rates in following paragraphs are spectrally *integrated* quantities. Easier said than done. Any of the absorption spectra in Chapter 2 or, closer to hand, Fig. 6.14, convey the unavoidable fact that Monte Carlo calculations – indeed, any calculations – of absorption at wavenumber intervals sufficiently small to resolve all absorption peaks and troughs over solar and terrestrial spectra would require computing time not measured in seconds, minutes, or even hours but days, weeks, months, years, possibly lifetimes. So we have to compromise and use absorption coefficients suitably averaged over a small number of bands: 32 solar bands, 12 terrestrial bands for the results in this section.

It is not irradiances *per se* that result in local atmospheric heating or cooling but rather their spatial rate of change, that is, solar and terrestrial flux divergences, which are shown in Fig. 6.21 for the irradiance profiles in Fig. 6.20. A negative flux divergence corresponds to heating (net transfer of radiant energy into a volume), a positive flux divergence corresponds to cooling (net transfer of radiant energy out of a volume). Almost all the action occurs in the lower 30 km of the atmosphere. Below about 15 km heating by absorption of solar radiation rapidly increases as does cooling by emission of terrestrial radiation. The two divergences are almost equal and opposite. The total flux divergence is shown on an expanded horizontal scale. Between about 8 km and 14 km the total flux divergence is positive, negative between about 8 km and the ground. The vertically integrated total flux divergence is negative because this profile is for a clear sky at solar noon.

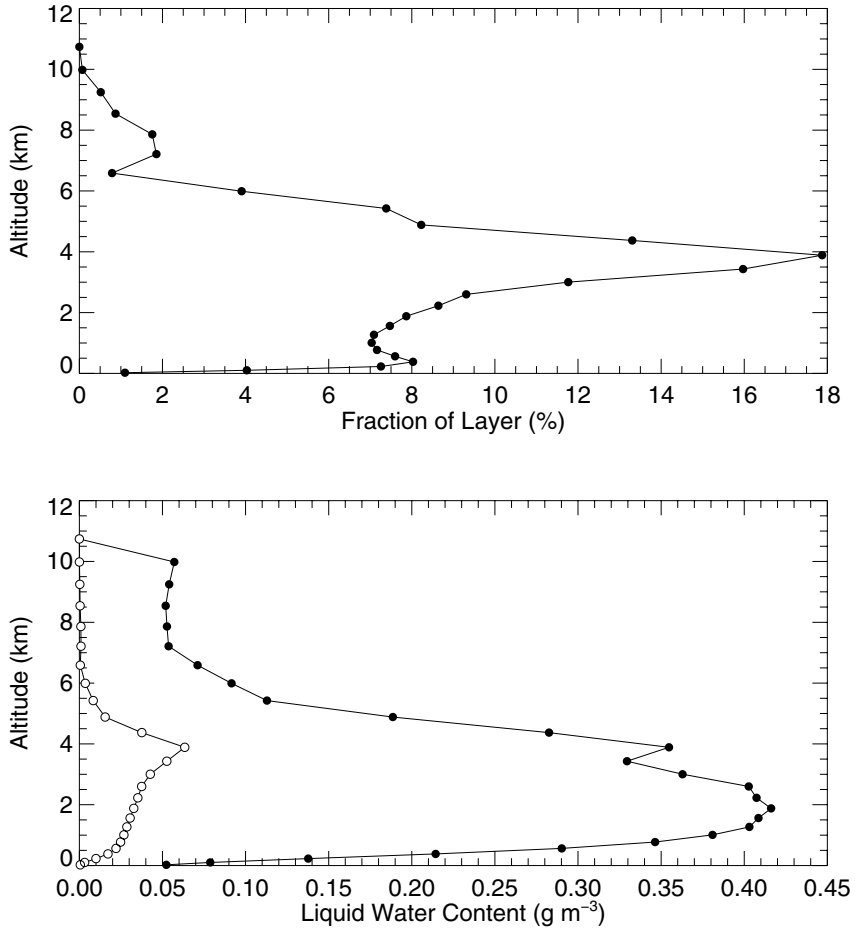

Figure 6.23: Liquid water profile for the cloud field depicted in Fig. 6.22. The top panel shows, for each layer (altitude) of boxes, the fraction of the total number of boxes that contains liquid water. The bottom panel shows the average liquid water content calculated two ways: an average over all boxes at each altitude (open circles); an average over only those boxes at each altitude that contain liquid water (closed circles).

Although the profiles in Figs. 6.20 and 6.21 were obtained by Monte Carlo calculations, they could have been obtained, and with much less time and effort, using any of the many methods for solving plane-parallel problems. Such methods, however, cannot be used to calculate profiles for a horizontally heterogeneous cloud field such as that shown in Fig. 6.22. This figure depicts by brightness differences (shading) horizontal variations in integrated liquid water content, obtained from model calculations, in a region 400 km on a side and 100 km deep

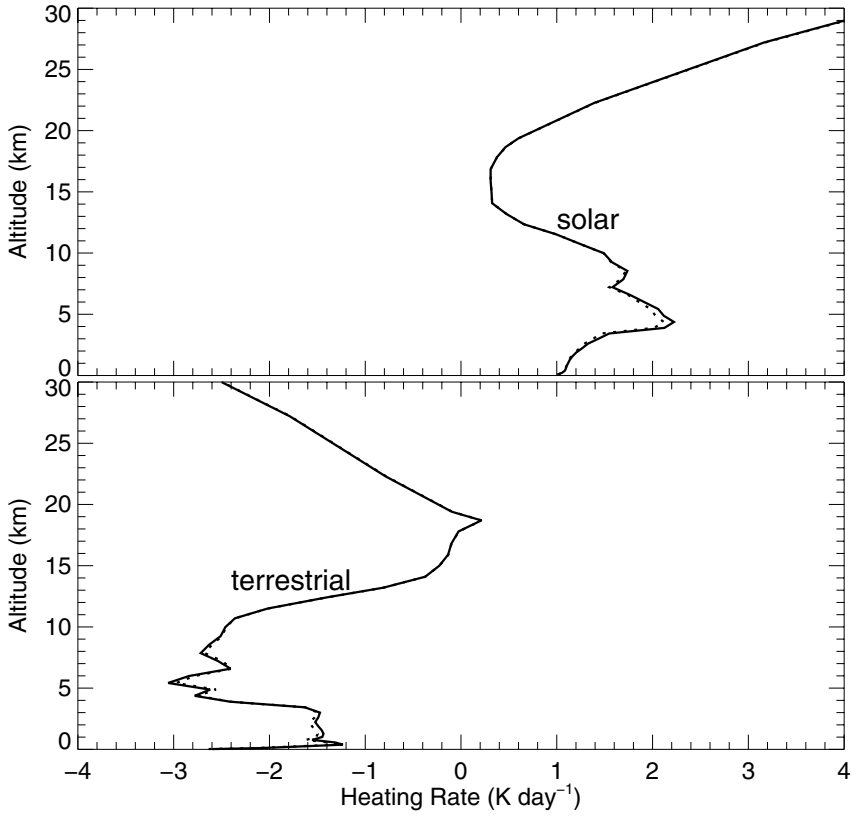

Figure 6.24: Horizontally averaged heating rates for solar (top) and terrestrial radiation (bottom) calculated by the Monte Carlo method for the cloud field depicted in Fig. 6.22. The solar zenith angle is 60° and the reflectivity of the diffusely reflecting ground is 0.2 at all solar wavelengths. The dots show results obtained from one-dimensional radiative transfer calculations in which each 2 km by 2 km vertical column with 44 levels is treated as infinite in lateral extent and an average calculated for the 40,000 vertical columns. Terrestrial radiation results from Cole (2005).

composed of 40,000 columns with 44 levels. Thus the region is subdivided into 1,760,000 rectangular boxes each 2 km on a side but with variable thicknesses because equal vertical distances do not correspond to equal masses. Fewer than about 4% of the boxes contain liquid water, and as evidenced by Fig. 6.22, the horizontal distribution of liquid water is not uniform. Figure 6.23 shows the vertical distribution of liquid water, which peaks at a few kilometers and vanishes above about 10 km.

Vertical heating rates, expressed as a rate of temperature change (assuming no net evaporation or condensation), arithmetically averaged at each altitude over the entire region, are shown in Fig. 6.24 for both solar and terrestrial radiation. For each of the 40,000 vertical columns with 44 levels profiles also were calculated by the Monte Carlo method treating each

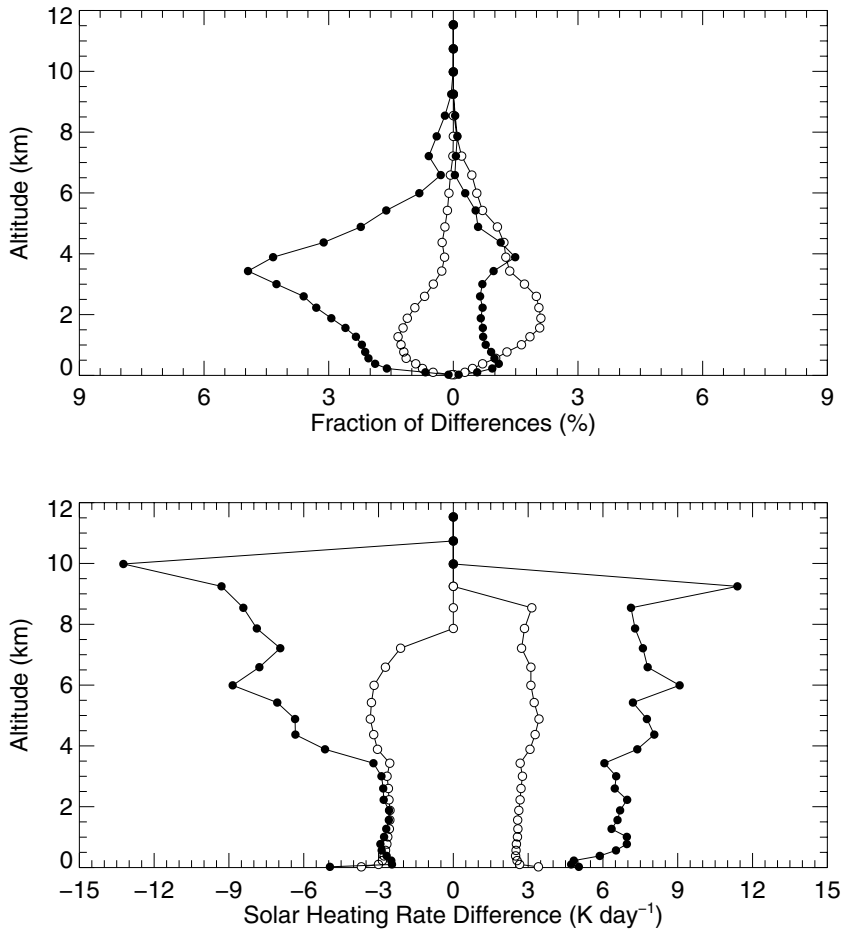

Figure 6.25: Fraction at each altitude of the total number of boxes with statistically significant differences between solar radiation heating rates computed by the Monte Carlo method applied to the full domain and applied to each vertical column as if it were infinite in lateral extent for the cloud field depicted in Fig. 6.22 (top). The arithmetic average of the significant heating rate differences for the boxes in each layer (bottom); the bin size is $0.5\,\mathrm{K\,day^{-1}}$. Solid circles are for boxes containing cloud liquid water, and open circles are for boxes with no liquid water.

column as if it were infinite in lateral extent, and hence independent of all other columns, then all these profiles arithmetically averaged. Agreement between the two profiles is surprisingly good – on average.

The Monte Carlo method is a statistical sampling technique that gives only *estimates* of quantities (e.g., heating rates) that in principle could be obtained by solving deterministic

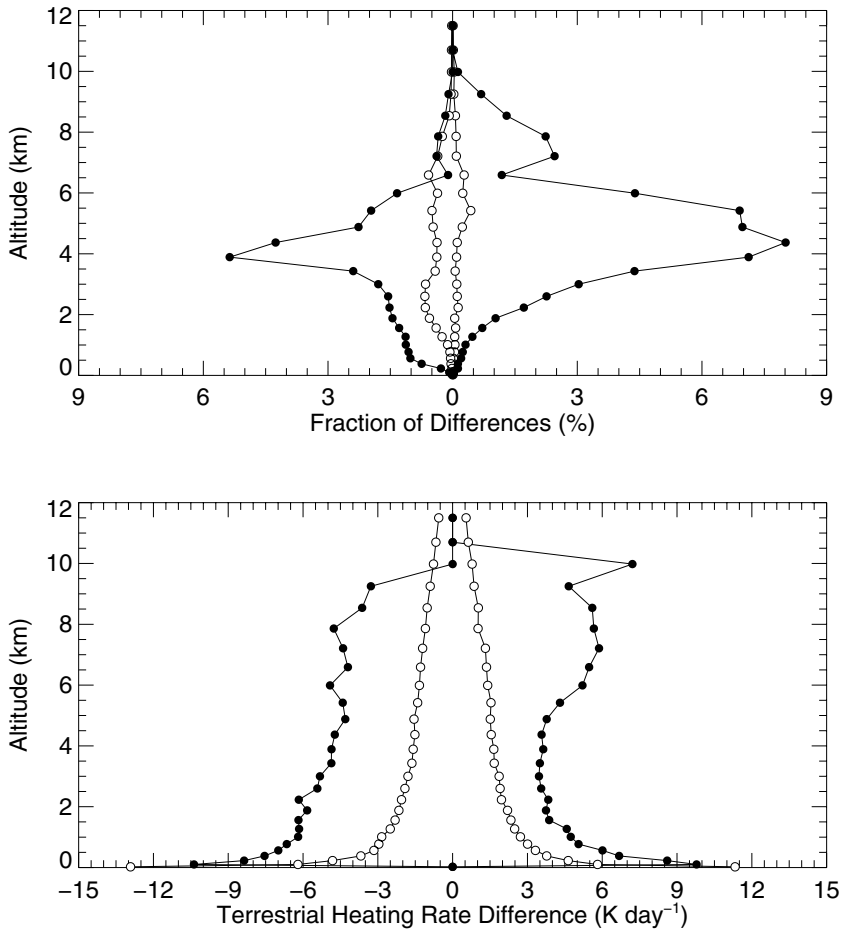

Figure 6.26: Fraction at each altitude of the total number of boxes with statistically significant differences between terrestrial radiation heating rates computed by the Monte Carlo method applied to the full domain and applied to each vertical column as if it were infinite in lateral extent for the cloud field depicted in Fig. 6.22 (top). The arithmetic average of the significant heating rate differences for the boxes in each layer (bottom); the bin size is $0.5\,\mathrm{K\,day^{-1}}$. Solid circles are for boxes containing cloud liquid water, and open circles are for boxes with no liquid water. Terrestrial radiation results provided by Jason Cole.

equations such as Eq. (6.15). Wherever there are estimates, uncertainties in their values are lurking in the background. A single Monte Carlo calculation gives an estimate, similar calculations give different estimates (see Fig. 6.3), and hence curves obtained from such calculations are plots of estimated *mean* values even if not explicitly noted. If one does a Monte

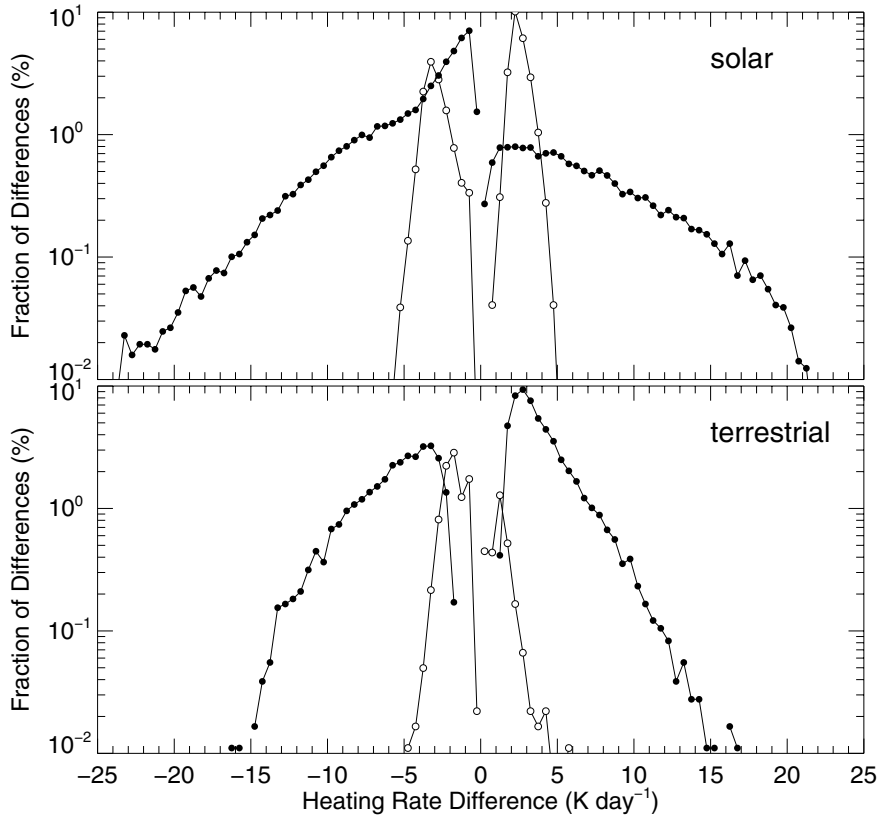

Figure 6.27: Fraction of the total number of boxes with statistically significant differences between radiative heating rates computed by the Monte Carlo method applied to the full domain and applied to each vertical column as if it were infinite in lateral extent for the cloud field depicted in Fig. 6.22. Solid circles are for boxes containing cloud liquid water, open circles are for boxes with no liquid water. The bin size is $0.5\,\mathrm{K\,day^{-1}}$. Terrestrial radiation results provided by Jason Cole.

Carlo calculation of, say, reflected irradiance by following the history of 10^8 photons, then does this again and again and again, each result will be slightly different. By doing several sets of such calculations, say 10 or more, one can calculate a mean and its standard deviation.

This was done to obtain the solar and terrestrial heating rate profiles (Fig. 6.24) for the heterogeneous cloud field depicted in Fig. 6.22. And the horizontally averaged heating rate profiles were surprisingly close – on average. But, how do the heating rates computed the two different ways compare from one box to the next? In each solar wavelength band 10^8 photons were injected at random points into the top (at 100 km) of the 400 km square cloud field; the solar zenith angle was 60°. A set of calculations was repeated 10 times and a heating rate mean and its standard deviation determined for each of the 1,760,000 boxes. Then we did 10

sets of Monte Carlo calculations for each of the 40,000 vertical columns taken to be infinite in lateral extent and with $10^8/4 \times 10^4 = 2.5 \times 10^3$ incident photons in each solar band and again computed a heating rate mean and standard deviation. Because Monte Carlo calculations give only estimated means with their standard deviations we have to decide whether a calculated difference for a box between the two calculations is statistically significant.

Let $\overline{Q}$ be the mean heating rate and σ its standard deviation for any of the 1,760,000 boxes calculated by assuming that each column is infinite in lateral extent. Let Q_c be the mean heating rate and σ_c its standard deviation for that same box calculated by the Monte Carlo method for the three-dimensional heterogeneous cloud field. If $\overline{Q} + 3\sigma < Q_\mathrm{c} + 3\sigma_\mathrm{c}$, we take the statistically significant difference to be $\overline{Q} - Q_\mathrm{c}$ (negative). If $\overline{Q} - 3\sigma > Q_\mathrm{c} + 3\sigma_\mathrm{c}$, we take the statistically significant difference to be $\overline{Q} - Q_\mathrm{c}$ (positive). Solar heating rate differences are statistically significant for 56,690 boxes, 35,761 in cloudy sky, 20,292 in clear sky, all below the highest cloudy boxes. Terrestrial heating rate differences are statistically significant for 18,098 boxes, 15,885 in cloudy sky, 2,213 in clear sky.

Figure 6.25 shows the vertical distribution of the solar heating rate differences for both cloudy and clear sky and Fig. 6.26 shows the vertical distribution of the terrestrial heating rate differences. Figure 6.27 shows how the statistically significant solar and terrestrial heating rate differences are apportioned over all boxes, those with and without cloud water. The conclusions to be drawn from all these figures are that although treating each column in a heterogeneous cloud field as if it were infinite in lateral extent and then averaging over all columns agrees well with the average for the three-dimensional cloud field, box by box differences can be large, are mostly below the highest clouds, are greater for cloudy than for clear regions, and greater for solar radiation than for terrestrial radiation. All of these results are expected on physical grounds: clouds throw a monkey wrench into one-dimensional calculations, the more so at solar wavelengths because scattering by clouds at these wavelengths is not negligible. The average over columns does not, in general, represent any particular box well. The extent to which this affects climate and weather prediction by models is difficult to say, a variation on the perennial question, Do many wrongs make a right?

References and Suggestions for Further Reading

The classic – a much overused word – treatise on radiative transfer is by Subrahmanyan Chandrasekhar, 1960: *Radiative Transfer*. Dover. This is mathematically formidable, not the first place for a neophyte to go to learn the rudiments. Less formidable are the two volumes by another of the giants of the field, Hendrick C. van de Hulst, 1980: *Multiple Light Scattering: Tables, Formulas, and Applications*. 2 Vols., Academic.

Two textbooks at about the same level as this one are Jacqueline Lenoble, 1993: *Atmospheric Radiative Transfer*. A. Deepak; Grant William Petty, 2004: *A First Course in Atmospheric Radiation*. Sundog Pub. More advanced textbooks are Gary E. Thomas and Knut Stamnes, 1999: *Radiative Transfer in the Atmosphere and Ocean*. Cambridge University Press, and K. N. Liou, 2002: *An Introduction to Atmospheric Radiation*, 2^{nd} ed., Academic Press.

For atmospheric radiative transfer applied to remote sensing see Graeme L. Stephens, 1994: *Remote Sensing of the Lower Atmosphere: An Introduction*. Oxford University Press.

Early papers by such household (if inhabited by astronomers) names as Schuster, Eddington, Schwarzschild, Rosseland and Milne are reprinted in Donald H. Menzel, 1966: *Selected Papers on Transfer of Radiation*. Dover.

One of the methods most widely used in atmospheric science for solving the one-dimensional radiative transfer equation for scattering and emitting media is described by Knut Stamnes, Si-Chee Tsay, Warren Wiscombe, and Kolf Jayaweera, 1988: Numerically stable algorithm for discrete-ordinate-method radiative transfer in multiple scattering and emitting layered media. *Applied Optics*, Vol. 27, pp. 2502–9.

Radiative transfer for which the diffusion approximation is adequate can take advantage of the great number of solutions to problems of diffusion of matter and of energy, for example, see Horatio S. Carslaw and John C. Jaeger, 1959: *Conduction of Heat in Solids*, 2^{nd} ed., Oxford , John Crank, 1975: *The Mathematics of Diffusion*, 2^{nd} ed., Oxford University Press.

Transport of neutrons is formally similar to transport of photons, and the diffusion approximation for neutrons has been used extensively for more than half a century in the design of nuclear reactors. For two good treatments of neutron diffusion theory see Samuel Glasstone and Milton C. Edlund, 1952: *The Elements of Nuclear Reactor Theory*. D. Van Nostrand, Ch. V; Robert V. Meghreblian and David K. Holmes, 1960: *Reactor Analysis*, McGraw-Hill, Ch. 5.

For a brief, elementary treatment of the Monte Carlo method (although not applied to radiative transfer) see I. M. Sobol', 1974: *The Monte Carlo Method*. University of Chicago Press. For an advanced treatise on this method applied to atmospheric radiation see Guri I. Marchuk., Gennadi A. Mikhailov, Magamedshafi A. Nazaraliev, Radzmik A. Darbinjan, Boris A. Kargin, and Boris S. Elepov, 1980: *The Monte Carlo Methods in Atmospheric Optics*. Springer.

For a clear discussion of the Monte Carlo method applied to engineering radiative transfer see Michael F. Modest, 1993: *Radiative Heat Transfer*. McGraw-Hill, Ch. 19. This book also has chapters on other methods for solving the radiative transfer equation in emitting and scattering media.

For more about subtracting the forward peak from angular scattering and reducing the scattering coefficient correspondingly (Sec. 5.3.2) see John F. Potter, 1970: The delta function approximation in radiative transfer theory. *Journal of the Atmospheric Sciences*, Vol. 27, pp. 943–9, and Warren J. Wiscombe, 1977: The delta-M method: Rapid yet accurate radiative flux calculations for strongly asymmetric phase functions. *Journal of the Atmospheric Sciences*, Vol. 34, pp. 1408–22.

For an application of the Monte Carlo method to the transport of radiation from lightning within a cloud see Larry W. Thomason and E. Philip Krider, 1982: The effects of clouds on the light produced by lightning. *Journal of the Atmospheric Sciences*, Vol. 39, pp. 2051–65.

The instrument used to make the irradiance measurements in Fig. 6.12 is described in Peter Pilewskie, John Pommier, Robert Bergstrom, Warren Gore, Steve Howard, Maura Rabbette, Beat Schmid, Peter V. Hobbs, and Si-Chee Tsay, 2003: Solar spectral radiative forcing during the Southern African Regional Science Initiative. *Journal of Geophysical Research*, Vol. 108, pp. 8486–92. The instrument used to measure droplet concentrations for deriving the liquid water content profile in Fig. 6.12 is described in Darrel Baumgardner, Haflidi Jonsson, William Dawson, Darren O'Connor, and R. Newton, 2001: The cloud, aerosol and precipitation spectrometer: A new instrument for cloud investigations, *Atmospheric Research*, Vol. 59, pp. 251–64. The experiment in which the measurements in Fig. 6.12 were obtained is described by Graham Feingold, Reinhold Furrer, Peter Pilewskie, Lorraine A. Remer, Qilong Min, and Haflidi Jonsson, 2005: Aerosol indirect effect studies at Southern Great Plains during the May 2003 intensive operations period: Optimal estimation of drop-size from multiple instruments. *Journal of Geophysical Research* (in press).

The Monte Carlo method for horizontally and vertically inhomogeneous media that emit and scatter, outlined in Section 6.3.5, is described in more detail by Jason N. S. Cole, 2005: Assessing the importance of unresolved cloud-radiation interactions in atmospheric global climate models using the multiscale modelling framework. Doctoral Thesis, Department of Meteorology, The Pennsylvania State University. Computer codes described in this thesis were used for the terrestrial radiation calculations shown in Figs. 6.20, 6.21, 6.24, 6.26 and 6.27.

The method within the atmospheric sciences in widest use for treating three-dimensional emitting and scattering media is by K. Franklin Evans, 1998: The spherical harmonics discrete ordinate method for three-dimensional atmospheric radiative transfer. *Journal of the Atmospheric Sciences*, Vol. 55, pp. 429–46.

The scheme for efficiently calculating radiances with the Monte Carlo method is discussed by K. Franklin Evans and Alexander Marshak, 2005: Numerical methods, in Alexander Marshak and Anthony B. Davis Eds., *3D Radiative Transfer in Cloudy Atmospheres*, Ch. 4, Springer.

Time-resolved radiative transfer is not a pipe dream, not only possible but with practical applications. For example, the shadow of an illuminated object embedded in a turbid medium is blurred because of multiply scattered radiation. But this radiation takes longer to reach a detector, and hence can be partly eliminated by ultrafast illumination and detection. See, for example, K. M. Yoo, B. B. Das, and R. R. Alfano, 1992: Imaging of a translucent object hidden in a highly scattering medium from the early portion of the diffuse component of a transmitted ultrafast laser pulse. *Optics Letters*, Vol. 17, pp. 958–60 and references cited therein.

For an overview of photon path lengths and their relevance to atmospheric radiative transfer see Graeme L. Stephens, Andrew K. Heidinger, and Philip M. Gabriel, 2005: Photon paths and cloud heterogeneity: An observational strategy to assess effects of 3D geometry on radiative transfer, in Alexander Marshak and Anthony B. Davis, Eds., *3D Radiative Transfer in Cloudy Atmospheres*, Ch. 13, Springer.

Some of the first surface-based instruments developed specifically for photon path length studies in clear and cloudy atmospheres are discussed by Klaus Pfeilsticker, Frank Erle, Oliver Funk, Hansjörg Veitel, and Ulrich Platt, 1998: First geometrical pathlengths probability density function derivation of the skylight from spectroscopically highly resolving oxygen A-band observations – 1. Measurement technique, atmospheric observations and model calculations. *Journal of Geophysical Research-Atmospheres*, Vol. 103, pp. 11483–504, and Qilong Min and Lee C. Harrison, 1999: Joint statistics of photon pathlength and cloud optical depth. *Geophysical Research Letters*, Vol. 26, pp. 1425–8.

The horizontally inhomogeneous cloud field depicted in Fig. 6.22 was obtained from model calculations by Wojciech W. Grabowski, Xiaoqing Wu, Mitchell W. Moncrieff, and William D. Hall, 1998: Cloud-Resolving modeling of cloud systems during Phase II of GATE. Part II. Effects of resolution and the third spatial dimension. *Journal of the Atmospheric Sciences*, Vol. 55, pp. 3264–82.

The moisture and temperature profiles used for the calculations in Fig. 6.20 are from Howard W. Barker and 31 co-authors, 2003: Assessing 1D atmospheric solar radiative transfer models: interpretation and handling of unresolved clouds. *Journal of Climate*, Vol. 16, pp. 2676–99.

What are called correlated-k methods often are used in atmospheric science for averaging over fine-structured absorption spectra to obtain broad-band absorption coefficients. The variation on this method used for the solar calculations in this chapter is from Seiji Kato, Thomas P. Ackerman, James H. Mather, and Eugene E. Clothiaux, 1999: The k-distribution method and correlated-k approximation for a shortwave radiative transfer model. *Journal of Quantitative Spectroscopy and Radiative Transfer*. Vol. 62, pp. 109–21. The method used at terrestrial wavelengths is that by Qiang Fu and Kuo-Nan Liou, 1992: On the correlated k-distribution method for radiative transfer in non-homogeneous atmospheres. *Journal of the Atmospheric Sciences*, Vol. 49, pp. 2139–56. Another variation on this method is by Eli Mlawer, Steven J. Taubman, Patrick D. Brown, Michael J. Iacono, and Shepard A. Clough, 1997: Radiative transfer for inhomogeneous atmospheres: RRTM, a validated correlated-k model for the longwave. *Journal of Geophysical Research-Atmospheres*, Vol. 102, pp. 16,663–82.

Correlated-k methods are not the only game in town for reducing the complexity of spectral calculations. For other methods see Andrew A. Lacis and James E. Hansen, 1974: A parameterization for the absorption of solar radiation in the Earth's atmosphere. *Journal of the Atmospheric Sciences*, Vol. 31, pp. 118–33 and Bruce P. Briegleb, 1992: Delta-Eddington approximation for solar radiation in the NCAR community climate model. *Journal of Geophysical Research-Atmospheres*, Vol. 97, pp. 7603–12.

Problems

6.1. To gain confidence that the N-stream equation [Eq. (6.2)] is correct (within the limits of the underlying approximations), show that it is correct for four streams. For simplicity

take two directions in the downward hemisphere, two in the upward hemisphere, and the cosines in the downward direction equal in magnitude but opposite in sign to those in the upward hemisphere. Don't forget that attenuation is along a direction of propagation, which corresponds to the z direction only for light directed upward or downward.

6.2. Show that the Henyey–Greenstein phase function [Eq. (6.59)] is normalized.

6.3. Verify Eq. (6.60).

HINT: This is perhaps done most easily by using the theorem for differentiation under the integral sign:

$$\frac{d}{da}\int f(a,x)\,dx = \int \frac{\partial f}{\partial a}\,dx,$$

where f and its partial derivative are continuous and the limits of integration do not depend on a.

6.4. For the phase function for scattering by a spherical dipole (Prob. 7.18), sometimes called the Rayleigh phase function, derive $\mu(\xi)$ in the same way that Eq. (6.64) is derived.

HINT: Cubic equations are exactly soluble.

6.5. Show that the vectors Eqs. (6.72)–(6.74) form an orthonormal, right-handed system.

6.6. Within the framework of the diffusion approximation, find the rate (volumetric) at which radiant energy is absorbed in an infinite, uniform, isotropic medium at any distance r from a point source (isotropic). A check on your solution is conservation of radiant energy: the rate of radiant energy from the source must be equal to the rate at which energy is absorbed in the entire medium.

HINT: The most difficult part of this problem is determining how to incorporate the point source as a boundary condition. Imagine a small spherical cavity to be carved out of the medium and determine the net rate at which radiant energy leaves the cavity in the limit as its radius approaches zero.

6.7. Use the result of the previous problem to determine the mean distance from the origin a photon travels (*not* the total path length of the photon) before it is absorbed. You can probably make a good guess at the answer without doing any calculations.

6.8. Derive the reflectivity of an infinite, plane-parallel, absorbing medium using diffusion theory and compare this reflectivity with Eq. (5.72) for the two-stream theory. By inspection of the diffusion theory reflectivity you should be able to give rough criteria (i.e., the range of medium properties) for when diffusion theory is definitely *not* a good approximation. After you have done so, try to obtain these criteria solely by physical arguments.

HINT: Reflectivities must be less than 1.

6.9. For what function, and only what function (of three space variables), is the directional derivative the same in all directions?

6.10. Equation (6.25) is a continuity equation for radiant energy. But it cannot be correct in general if the radiation field is explicitly time-dependent. Derive a more general form of this continuity equation. Why is it not, in general, identical in form to the continuity equation in fluid mechanics? When is it identical and why?

HINTS: Use the definition of the vector irradiance, the divergence theorem, and the same kinds of arguments used to derive the continuity equation of fluid mechanics.

6.11. The continuity equation derived in the previous problem is completely general. It does not depend on the equation of radiation transfer Eq. (6.15). To the contrary, this equation must be consistent with the continuity equation, and as it stands it is not. What time-dependent term must be added to the left side of Eq. (6.15) so that it is consistent with the general continuity equation?

6.12. Beginning with the general continuity equation obtained in Problem 6.10, derive a time-dependent diffusion equation for photons. Consider the special case of no absorption. Have you seen this equation before?

6.13. It is not necessary to solve a differential equation in order to obtain some insight from it. For example, beginning with the diffusion equation derived in Problem 6.12 for a nonabsorbing medium you should be able to answer the following question. Suppose that a plane-parallel medium is suddenly illuminated at its upper boundary. Everything takes time. Approximately how long after the illumination is turned on will the medium at a distance h from the boundary be illuminated? If your answer is not what might be expected at first glance, explain.

HINT: This problem entails what the fluid mechanics folks call scale analysis.

6.14. Consider a cylindrical medium of radius a extending from $z = 0$ to ∞. The scattering and absorption properties of the medium are uniform and it is illuminated by a uniform and isotropic source at $z = 0$. The medium is surrounded by empty space, which means that no photons that leak out the sides can return. Using the diffusion approximation, find the rate at which irradiance is attenuated deep within the medium. By deep is meant that z is sufficiently large that attenuation is dominated by a *single* exponential term. Compare this attenuation rate with that for the same medium but infinite in lateral extent ($a \to \infty$). Interpret your result physically. Also, consider the limiting case in which the medium is nonabsorbing.

HINT: This is an advanced problem. To solve it requires knowing how to solve partial differential equations in more than one variable using the method of separation of variables. An outline of the solution is given by Craig F. Bohren and Bruce R. Barkstrom, 1974: Theory of the optical properties of snow. *Journal of Geophysical Research*, Vol. 79, pp. 4527–35.

6.15. If you assume that the area of a circle is proportional to the area of the square that circumscribes it, you can estimate the value of π by generating many points randomly in a square with side one unit long and counting the fraction of points that lie within the circle. Try it.

6.16. By computations similar to those used to obtain π in Problem 6.15 you can estimate the circumference of a circle. Does an additional source of error enter into the estimate for this problem that is absent from Problem 6.15?

6.17. To do Problems 6.20, 6.21, and 6.22 you need a correct algorithm for choosing source points at random on a circular disc. You might think that the way to do this is to choose cylindrical polar coordinates (r, φ) at random. That is, choose r by picking a random number between 0 and 1 (the disc has radius 1) and φ by choosing a random number between 0 and 1 and multiplying it by 2π. Try this. Plot enough points to see a pattern. It is not likely to look random. Why? Can you come up with an algorithm (or even two) that does result in a distribution of points on the disc that at least looks random?

6.18. Use the expression for a small solid angle in spherical coordinates to derive Eq. (6.80). It may be easier to derive this result by considering isotropic emission by a surface.

6.19. Derive equations Eqs. (6.82) and (6.83). Write a Monte Carlo code that demonstrates that these equations do indeed produce the correct distributions.

6.20. Redo Problem 4.63 using the Monte Carlo method to determine the (average) irradiance at any depth z in the black tube. Compare your computational results with the (approximate) analytical expression obtained in that problem.

6.21. As a variation on Problem 6.20, suppose that the walls of the tube are specularly reflecting with a reflectivity less than 100%. For simplicity take this reflectivity to be independent of direction of incidence. Again, determine the average irradiance at a depth z in the tube as a function of reflectivity.

6.22. As a variation on Problem 6.20, suppose that the walls of the tube are diffusely reflecting with a reflectivity less than 100%. For simplicity take this reflectivity to be independent of direction of incidence. Again, determine the average irradiance at a depth z in the tube as a function of reflectivity.

6.23. Within the framework of diffusion theory, find the angular dependence of the radiance reflected by an infinite, absorbing, plane-parallel medium illuminated by irradiance F_0.

6.24. Within the framework of diffusion theory, find the angular dependence of the radiance reflected by a finite, nonabsorbing, plane-parallel medium overlying a medium with an absorptivity of 1 and illuminated by irradiance F_0.

6.25. Suppose that you propose to measure absorption by a medium by measuring the angular dependence of the reflected radiance from it. You argue that the greater the slope of the radiance (relative to the radiance at $\vartheta = \pi/2$) versus $\cos\vartheta$, the more absorbing the medium. Based on inspection of the solution to the two previous diffusion theory problems, what is one of the major drawbacks to your idea?

6.26. The two-stream theory is fundamentally incapable of yielding reflected radiances. What we often do, therefore, is assume that the radiance is isotropic and hence can be obtained from the irradiance. The diffusion approximation is not quite so limited, but can at best yield only an approximate radiance of simple form. Because of these limitations of the two (similar) theories, explain why they are not likely to give good results for optically thin, negligibly absorbing media and for strongly absorbing media.

6.27. Show that within the framework of the diffusion approximation it would be possible to infer ground albedo under a completely overcast sky by measuring the (relative) slope of the curve of radiance versus cosine of the radiance zenith angle (equivalent to the angle between the downward directed normal at cloud base and the direction of the radiance as it leaves the bottom of the cloud). Assume that the clouds are nonabsorbing. This problem was inspired by a discussion on pages 653–4 of Hendrik C. van de Hulst, 1980: *Multiple Light Scattering: Tables, Formulas, and Applications*. Vol. 2, Academic, who in turn was inspired by work (in Russian) by K. S. Shifrin and D. A. Kozhaev.

6.28. The equation of transfer in Section 6.1.2 is for incoherent scattering. We pointed out in Section 3.4.8 that scattering in the exact forward direction by two (or more) particles is in phase regardless of their separation. Thus the theory in this chapter is not applicable to

this direction. And the same is true, although perhaps not as obvious, for the exact backward direction. Even multiple scattering by a suspension of randomly distributed particles can give rise to *coherent backscattering*. This has essentially nothing to do with the glory (Sec. 8.4.3) because coherent backscattering can be obtained with particles too small to yield the glory. What is special about the backward direction such that multiply scattered waves can interfere constructively for this direction regardless of the number of scatterings and the separation of the scatterers?

HINT: A sketch of various rays scattered by two or more scatterers is essential as is invoking time reversal (Sec. 1.3). A simple figure is all that is needed. For a good expository article see R. Corey, M. Kissner, and P. Saulnier, 1995: Coherent backscattering of light. *American Journal of Physics*, Vol. 63, pp. 560–4.

6.29. In Problem 6.28, what is the ratio of the radiance in the exact backscattering direction taking into account coherent backscattering relative to the radiance in this direction assuming complete incoherence? What is the error in the reflected irradiance as a result of ignoring coherent backscattering? Is this error of any consequence for irradiances given that the angular region of coherent backscattering is a few mrad.

HINT: For the second part of this problem assume that the incoherent reflected radiance is constant and that the coherent reflected radiance is constant everywhere and equal to the incoherent value except within an angle δ of the backward direction, where it is equal to the value determined in the first part of this problem.

6.30. According to the two-stream equations in Section 5.2 for a nonabsorbing medium, the net irradiance (difference between upward and downward irradiances) is the same for every altitude z. Show that this is a general result for any plane-parallel, nonabsorbing medium.

HINT: Use the equation satisfied by the vector irradiance and the divergence theorem.

6.31. Figure 6.15 shows Monte Carlo calculations of the relative difference in radiances at two closely-spaced frequencies in the near infrared (around 770 nm). The absorption optical thickness is 0.11 at one frequency (moderate absorption), but much smaller at the other frequency (weak absorption). Show that this relative difference for both the upward radiance at the top of the clear atmosphere and the downward radiance at the bottom is approximately equal to the negative of the absorption optical thickness. Does this result square with the detailed Monte Carlo calculations?

HINTS: No elaborate derivation is necessary. Assume negligible multiple scattering. You can derive the radiances by evaluating a path integral of radiance similar to Eq. (8.3) with the addition of absorption. Assume the uniform atmosphere approximation of Section 8.1.1. Both the scattering optical thickness and absorption optical thickness are $\ll 1$.

6.32. According to Fig. 6.20 the upward irradiance for a clear sky is approximately constant with altitude for the infrared part of the solar spectrum but increases slightly with altitude for the combined visible and ultraviolet. Try to explain this by physical arguments. You can check your intuition with the two-stream theory of Section 5.2.

6.33. Show, using the two-stream theory, that the relative values of the upward and downward radiances in Fig. 6.19 for the cloud with the smallest aspect ratio are plausible.

6.34. Explain the sudden rise in the heating rate by solar radiation at altitudes greater than about 20 km in Fig. 6.24.

6.35. We state in Section 6.3.5 that at terrestrial temperatures emission at visible and near-visible wavelengths is exceedingly small. To support this statement determine the ratio of spectral emission at the long-wavelength end of the solar spectrum (often taken to be $2.5\,\mu\mathrm{m}$) to emission at the middle of the terrestrial spectrum (often taken to be $10\,\mu\mathrm{m}$) at terrestrial temperatures.

6.36. Write a Monte Carlo program for investigating absorption by a cloudy sphere, large compared with the wavelength. See Problem 5.57.

6.37. Why are the Monte Carlo method upward and downward irradiances near cloud top [see Fig. 6.10 (bottom) and Fig. 6.11] greater than the incident irradiance and why does the two-stream theory not predict this?